Appl. Phys. B 58, 347–363 (1994)

Applied Physics B Lasers and Optics

Ultrafast All-Solid-State Laser Technology

U. Keller

Institute of Quantum Electronics, Swiss Federal Institute of Technology (ETH), CH-8093 Zürich, Switzerland
(Fax: +41-1/3712072, e-mail: Keller @ iqe.phys.ethz.ch)

Received 22 February 1994/Accepted 1 March 1994

Abstract. Passively mode-locked diode-pumped solid-state lasers can provide practical high-power laser sources with pico- and femtosecond pulse durations. We use semiconductors not only to optically pump but also to cw mode-lock or Q-switch a solid-state laser. A novel saturable absorber design, the Antiresonant Fabry-Perot Saturable Absorber (A–FPSA), allows of using semiconductor saturable-absorber materials even though they are generally not well-matched to the characteristics required for diode-pumped solid-state lasers, i.e., the semiconductors tend to have too much optical loss, a too low saturation intensity, and a too low damage threshold. This paper gives an overview of passively mode-locked ion-doped crystalline solid-state lasers. In particular, we present a quantitative discussion of A–FPSA mode locking, and compare A–FPSA mode locking with other passive mode locking techniques such as KLM (Kerr Lens Mode locking).

PACS: 42.55R, 42.65, 42.80

The goal of an all-solid-state laser technology is motivating many research efforts world-wide. The replacement of the gas-filled lamps typically used to pump solid-state crystalline lasers with high-power diode lasers, which can be precisely tuned to match the absorption of many solid-state lasers, results in very efficient pump sources and more compact, reliable lasers with other benefits such as simpler and reduced utility requirements. This technology allows of new applications in areas ranging from materials research and processing to medical diagnostics and surgery.

Our research is pushing the goal of an all-solid-state laser technology even further with the development of semiconductor passive-control elements for short-pulse generation. Passively mode-locked diode-pumped solid-state lasers have a great potential to become practical ultrafast laser sources with high average power (≥ 1 W) and high pulse-repetition rates. We use semiconductors not only to optically pump but also to cw mode-lock or Q-switch a solid-state laser. To generate ultrafast pulses passively, a saturable absorber with a fast recovery time is required for solid-state lasers. We use novel semiconductor devices, for which we can custom-engineer the appropriate physical parameters, such as saturation intensity, absorption wavelength, losses, impulse response, etc. due to the availability of advanced Molecular-Beam-Epitaxy (MBE) technology. Depending on the design parameters, these control elements can be used as passive Q-switchers or mode-lockers, and the resulting pulses range from the microsecond to the femtosecond regime.

Normally, however, semiconductor materials are not well-matched to the characteristics required for diode-pumped solid-state lasers, i.e., the semiconductors tend to have too much optical loss, a too low saturation intensity, and a too low damage threshold for typical solid-state lasers such as Nd:YAG. These issues are solved by use of the recently-developed A–FPSA [1] (Antiresonant Fabry-Perot Saturable Absorber), which integrates the semiconductor saturable absorber inside a Fabry-Perot cavity that is operated at antiresonance. Antiresonance means that the intensity inside the Fabry-Perot is smaller than the incident intensity, which decreases the device loss and increases the saturation intensity. The damage threshold is determined by the top reflector which is typically an evaporated dielectric mirror similar to other mirrors inside the laser cavity.

The A–FPSA is a nonlinear mirror, typically ≈ 400 μm thick, which simply replaces one of the laser-cavity end mirrors to passively mode-lock a cw pumped laser. This A–FPSA (Fig. 4a) has passively mode-locked successfully many different Nd-doped solid-state lasers such as Nd:YLF [1, 2], Nd:YAG [2, 3], Nd:fiber [4] and Nd:glass [5, 6] lasers with ps to sub-100 fs pulses. So far, the A–FPSA is the only intracavity saturable absorber in an all-solid-state ultrafast laser technology for which the mode locking is always self-starting and stable against Q-switching. The main reason is that the operation parameters, such as saturation intensity, losses, and impulse response of the A–FPSA can be custom-designed and adapted to the requirements of solid-state lasers.

A full theoretical understanding of the laser dynamics using a bitemporal A–FPSA is in progress. The results of this research should be a basic understanding allowing of optimization of these devices and extension to lasers at key wavelengths such as 850 nm, 1.3 μm, 1.55 μm, and 2 μm. The ultimate practicability of solid-state control elements for pulsed lasers should allow of new generations of compact reliable pulsed solid-state lasers, opening many new possible applications and uses of such ultrafast laser systems.

1 Historical Background: Revolution in Ultrashort-Pulse Generation

The commercial availability of high-power semiconductor (diode) lasers in the early 1980's lead to a major technology leap for solid-state lasers – the replacement of gas-filled flash or arc lamps used to excite the solid-state laser material, with diode lasers [7]. This resulted in a number of technical improvements. First, diode lasers have lifetimes of greater than 10000 h compared to lifetimes of several hundreds of hours for lamps. This means that lasers with much longer lifetimes and lower service requirements can be built. Because the wavelength of diode lasers can be precisely adjusted to match the absorption bands of many typical solid-state lasers (for example, Nd:YAG absorbs at 810 nm ± 1 nm), very efficient and compact lasers can be designed. Also, typical diode-pumped solid-state laser generate frequency-coherent light with very good diffraction-limited (TEM_{00}) spatial quality compared to the frequency incoherence and poor spatial quality typical for high-power diode laser arrays. A highly efficient cw diode-end-pumped Nd:YAG laser has been demonstrated with 60 W average power in a TEM_{00} mode and >90 W average power in multimode operation [8], for example. Thus, these new diode-pumped solid-state lasers offer performance characteristics not possible with any other laser technology.

The revolution in ultrashort-pulse generation with solid-state lasers was rooted in materials research of laser media in the late 1970's and early 1980's leading to the demonstration of the continuous-wave (cw) Ti:Sapphire laser in 1982 [9, 10]. This solid-state laser had the necessary bandwidth for amplification (i.e., 670 nm to 1100 nm) to support femtosecond-pulse generation. This material shows absorption at green wavelengths (≈550 nm or smaller) which is not yet possible to achieve directly with diode lasers. To allow for laser-diode pumping, additional broadband solid-state materials such as Cr:LiSAF have been developed [11, 12]. The research efforts to find new solid-state laser materials is still very active and ongoing.

The excellent optical and thermal properties of the Ti:Sapphire laser and its early availability as a commercial product in 1989 was the trigger for the "revolution" in ultrashort laser physics [13, 14], which was previously dominated by dye lasers (Fig. 1). Only three years after the Ti:Sapphire laser's introduction, many new mode-locking techniques had been discovered and demonstrated. The latest world-record in ultrashort-pulse generation directly from a laser, around 11 fs pulse width, was obtained in 1993 independently by two research groups [15, 16].

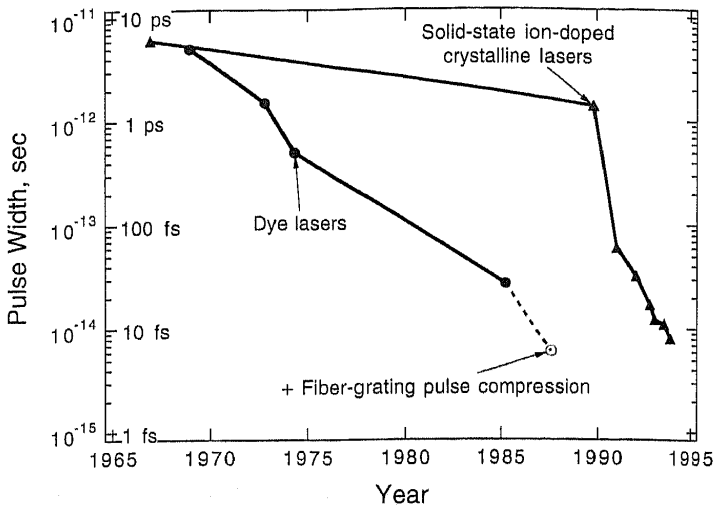

Fig. 1. Revolution in ultrafast laser technology. New solid-state lasers such as Ti:Sapphire lasers using novel mode-locking techniques generate ≈10 fs pulses direct out of the laser with >100 mW of average output power. A CPM dye laser produced pulses as short as 27 sf with ≈1 mW of average output power [81]. Only with external fiber grating pulse compression pulses as short as 6 fs were generated [82]

Table 1. Gain cross section σ_g, and the laser's upper-state lifetime τ_2 (i.e., fluorescent lifetime of the upper laser niveau). The product $\sigma_g\tau_2$ is a figure of merit for an efficient laser because the threshold pump power is inversely proportional $\sigma_g\tau_2$. Consequently, a small σ_g will generally require a long τ_2.

Laser material	Gain cross section	Upper-state lifetime
Semiconductors	$\approx 10^{-14}$ cm^2	≈1 ns
Dyes	$\approx 10^{-16}$ cm^2	≈10 ns
Ti:Sapphire	3.8×10^{-19} cm^2	2.5 μs
Nd:YAG (1.06 μm)	6.5×10^{-19} cm^2	250 μs
Nd:YLF (1.047 μm)	1.8×10^{-19} cm^2	450 μs
Nd:glass (phosphate)	4×10^{-20} cm^2	350 μs

New mode-locking techniques are necessary for Ti:Sapphire and other solid-state laser materials because their gain cross sections for stimulated laser emission σ_g are approximately 1000 times smaller than for dye lasers (Table 1). The product $\sigma_g\tau_2$, where τ_2 is the laser's upper-state lifetime, is a figure of merit for an efficient laser because the pump threshold is proportional to $(\sigma_g\tau_2)^{-1}$. Therefore, a small gain cross section generally requires a longer upper-state lifetime (Table 1). A long upper-state lifetime means that pulse-to-pulse dynamic gain saturation of the laser medium is negligible and does not support pulse formation. Thus, a fast saturable absorber is required to support short pulses. Such an effective fast saturable absorber, Kerr-Lens Mode locking (KLM), was discovered in 1990 by Spence et al. [17], which triggered a world-wide research activity to explain and expand their results [14, 18–20]. The 11 fs pulse-width world record mentioned earlier was obtained with KLM.

Previously, because of the lack of a suitable fast intracavity saturable absorber, the Ti:Sapphire laser was mode-locked with coupled cavity mode-locking techniques such as Additive Pulse Mode locking (APM) [21–24] using a reactive nonlinear coupled cavity with a fiber, and coupled-cavity Resonant Passive Mode locking (RPM) [25, 26] using an amplitude nonlinearity. The interest in coupled-cavity mode locking schemes declined very soon after the discovery of KLM which was a much simpler technique and generally produced shorter pulses with superior stability [27, 28]. The high average power of KLM Ti:Sapphire laser drastically improved the performance of synchronously pumped femtosecond OPOs (Optical Parametric Oscillators) providing tunable femtosecond pulses from the visible to the infrared [29].

Significant new progress has also been made in femtosecond fiber lasers with pulses as short as 38 fs [30]. However, femtosecond fiber lasers typically produce low average power (< 10 mW) because the peak intensity and the pulse energy density tend to saturate the saturable absorber very fast or cause soliton instabilities. New techniques based on stretched-pulse additive-pulse mode locking [31] produced sub-100 fs pulses at a higher average power of 24 mW [32]. A more detailed discussion of these all-solid-state laser sources is beyond the scope of this paper, which puts the emphasis on bulk lasers with potentially much higher average output powers.

2 Kerr Lens Mode Locking

The KLM method relies on self-focusing of the laser beam due to the Kerr effect in the gain medium to guide the laser beam at high intensity more efficiently through an aperture within the laser cavity. This saturable absorber is not produced by the Kerr effect alone, but together with an aperture, producing lower loss for higher pulse intensities [18, 19] (Fig. 2). This saturable absorber is very fast, since the Kerr effect is produced by electronic polarization in the laser crystal resulting in a response time estimated to lie in the femtosecond regime.

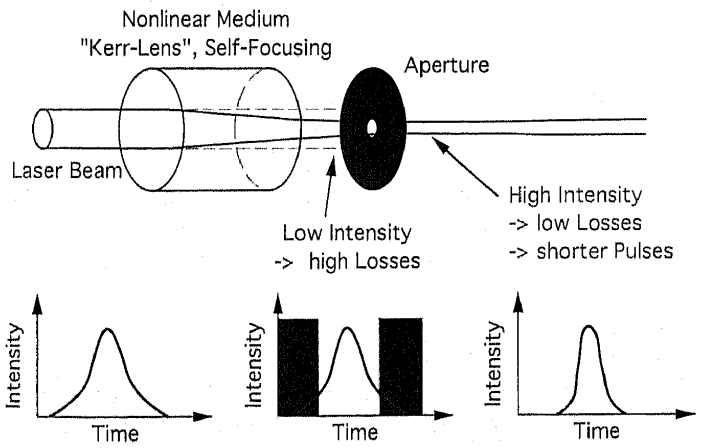

Fig. 2. Kerr Lens Mode locking (KLM) using a hard intracavity aperture. An effective fast saturable absorber is formed because the high-intensity part of the pulse has lower losses than the low-intensity part. The Kerr effect produces an intensity dependent lens due to an intensity dependent refractive index $\Delta n = \gamma I$ which focuses the high-intensity part of the laser beam more strongly through the aperture. The Kerr effect is a non-resonant nonlinearity with an estimated response time in the femtosecond regime and only a weak wavelength dependence enabling ultrashort pulse generation

Even without a hard intracavity aperture, self-focusing can produce a nonlinear gain increase if the gain varies spatially as for laser-pumped solid-state lasers [33]. As we will discuss later, especially in the picosecond regime, KLM is much smaller than the nonlinear reflectivity change of an A–FPSA.

The round trip small-signal gain coefficient g_0 in a laser-pumped cavity depends on the overlap of the cavity mode with the pump beam and is given by [34]

$$g_0 = \frac{P}{P_{\text{th}}} g_{0,\text{th}} \sim \frac{1}{A_l + A_p} \tag{1}$$

where A_l is the laser cavity mode area, A_p is the pump area inside the laser gain material, P the pump power, P_{th} the threshold pump power, and $g_{0,\text{th}}$ the round trip small-signal gain coefficient at threshold. Equation (1) assumes constant A_l and A_p through the gain medium. The unsaturated gain coefficient then determines the round-trip gain $G = \exp(g)$ and the round-trip saturated gain coefficient g:

$$G \equiv \exp(g) = \exp\left(\frac{g_0}{1 + \dfrac{I}{I_{\text{sat},g}}}\right) \tag{2}$$

where $I_{\text{sat},g}$ is the cw saturation intensity of the gain medium:

$$I_{\text{sat},g} = h\nu/\sigma_g \tau_2, \tag{3}$$

and $h\nu$ is the photon energy, σ_g is the gain cross section, and τ_2 is the upper state lifetime of the gain medium. At steady state the saturated gain equals the total laser loss:

$$G_{\text{tot}} = \exp(g - l) = 1 \Leftrightarrow g = l, \tag{4}$$

where l is the total round-trip loss coefficient. Similar to hard-aperture KLM, self-focusing produces a mode-size reduction ΔA_l and an increase of the intensity in the gain medium. Therefore, the gain is more strongly saturated by the short pulses than by cw oscillations (2), which discriminates at steady state against cw oscillations that do not reach threshold in the pulse-saturated laser cavity. In addition, the effective fast saturable absorber due to mode size reduction (1) discriminates instantaneously against cw oscillations. This "gain aperturing" can be sufficient to form a fast saturable absorber. The gain difference Δg between the pulsed operation and the cw oscillations in the pulse-saturated laser cavity $I_{\text{pulsed}}/I_{\text{sat},g}$ is given by:

$$\Delta g = g_{\text{pulsed}} - g_{\text{cw}} = \frac{g_{0,\text{pulsed}} - g_{0,\text{cw}}}{1 + \dfrac{I_{\text{pulsed}}}{I_{\text{sat},g}}}, \tag{5}$$

where I_{pulsed} is the average intensity inside the gain medium at pulsed laser operation. With (1) and the steady-state condition that g_{pulsed} is equal to l follows for "gain aperturing" KLM:

$$\frac{\Delta g}{l} = \frac{A_{l,\text{pulsed}} - A_{l,\text{cw}}}{A_{l,\text{cw}} + A_p} = \frac{-\Delta A_l}{A_{l,\text{cw}} + A_p}, \quad (6)$$

where $A_{l,\text{cw}}$ is the mode size in the laser crystal in the cw cavity, $\Delta A_l = A_{l,\text{pulsed}} - A_{l,\text{cw}}$ is the mode-size reduction due to self-focusing which can be determined with ABCD matrix calculations [20, 35]. For $\Delta A_l < 0$ self-focusing produces an effective fast saturable absorber with $\Delta g > 0$. Gain aperturing is sufficiently large for femtosecond pulse duration and when the laser cavity is operated near the stability limit. For example, the world record of 11 fs is based on KLM with gain aperturing [15].

KLM has become a very successful and broadly used mode-locking technique for femtosecond solid-state lasers. However, KLM has also some significant disadvantages compared to other mode-locking techniques. One is the weak starting mechanism for the mode-locking process [18], because self-focusing becomes important only at high peak intensities. Thus, the normal fluctuations due to laser noise in continuously pumped lasers are typically not intense enough to start pulse generation with KLM. Self-starting KLM Ti:Sapphire lasers have been demonstrated under certain cavity designs operated close to the cavity stability limit [36, 37]. To initiate more reliable self-starting for a broad range of cavity designs one of several techniques are used: intracavity dye saturable absorber [38, 39], RPM [18], acousto-optic modulators [40, 41, 42], shaking mirrors [43], and synchronous pumping [44]. All of these techniques basically amplify the effect of initial noise bursts in the laser to get the pulse formation started. However, these starting mechanisms either increase the complexity and cost of the laser or are not practical for industrial applications. In addition, KLM is rather weak for picosecond pulse generation and generally not sufficient for stable reliable mode locking. Therefore, it would be desirable to have another solid-state saturable absorber which fulfills all the requirements for solid-state lasers and removes the limitations of KLM.

3 Antiresonant Fabry-Perot Saturable Absorber (A–FPSA)

Semiconductor saturable absorbers have the advantage that they provide a compact bulk nonlinearity without any critical alignment, and that their bandgap wavelength and their nonlinearity can be custom-designed with bandgap engineering. They have previously mode-locked diode [45–47] and color-center [48] lasers. However, in rare-earth (i.e., Nd:YLF) and transition-metal (i.e., Ti:Sapphire) solid-state lasers, intracavity semiconductors introduce too much loss, have a too small saturation intensity and have problems withstanding the high intracavity peak intensities. Also, the long upper-state lifetime of many solid-state lasers (Table 1) increases the tendency of the laser to self-Q-switching (see Sect. 7). The saturation intensity of the semiconductor saturable absorber needs to be sufficiently high such that the absorption is not already bleached at cw intensities. Thus, the laser can lower its losses by going into a pulsed mode of operation where the saturable absorber is more strongly bleached.

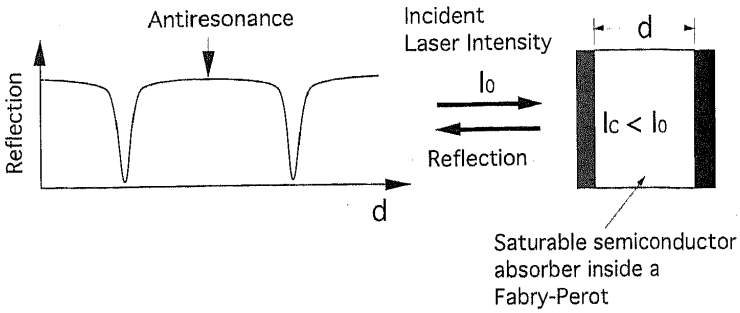

Fig. 3. An Antiresonant Fabry-Perot Saturable Absorber (A–FPSA) integrates the saturable absorber inside a Fabry-Perot cavity with a large free spectral range. Antiresonance transforms the saturable absorber to a device with low loss, high saturation intensity, and low damage threshold, because the intensity inside the Fabry-Perot I_c is always much smaller than the incident intensity I_0. The top reflector is typically an evaporated dielectric SiO_2/TiO_2 mirror

Our solution was the invention of the Antiresonant Fabry-Perot Saturable Absorber (A–FPSA) [1] where the semiconductor saturable absorber is integrated inside a Fabry-Perot which is operated at antiresonance (Fig. 3). At antiresonance the intensity inside the Fabry-Perot cavity is always smaller than the incident intensity, which increases the effective saturation intensity (observed before the top mirror) and the damage threshold of the device. Therefore, the antiresonance transforms the semiconductor saturable absorber to a device with high saturation intensity, low losses (top reflector typically $\approx 95\%$), and low damage threshold (top reflector is typically a TiO_2/SiO_2 dielectric mirror), as required for solid-state lasers.

An A–FPSA designed for Nd-doped lasers operating near a wavelength of 1.05 μm (Fig. 4a) uses a low-temperature MBE-grown (i.e., 380° C) InGaAs/GaAs saturable absorber [49] with a bandgap wavelength at ≈ 1.05 μm (Fig. 4b, trace 1). The low-intensity reflectivity measurements of the AR-coated A–FPSA (Fig. 4b, trace 2) and the A–FPSA (Fig. 4b, trace 1) sample clearly show that the Fabry-Perot is operated in the range of antiresonance. In addition, we grew simultaneously a reference saturable absorber sample directly on a GaAs wafer without the bottom reflector (Fig. 4b, trace 3). The final A–FPSA (Fig. 4b, trace 1) has a high reflectivity bandwidth of ≈ 70 nm limited by the lower GaAs/AlAs mirror. Such an A–FPSA can support femtosecond pulse durations because the group-delay dispersion at antiresonance is near zero with only a small variation of < 0.5 fs within a 70 nm bandwidth.

The A–FPSA usually has negligible bandwidth limitations at antiresonance, because the free spectral range is much larger than the gain bandwidth of many solid-state lasers. Additionally, the antiresonance operation is insensitive to thermal loading, and provides loose design tolerances. In contrast, a Fabry-Perot saturable absorber operated at resonance has a higher intensity inside the Fabry-Perot cavity, has very critical design tolerances, and can exhibit bistability effects, which are all detrimental for our application.

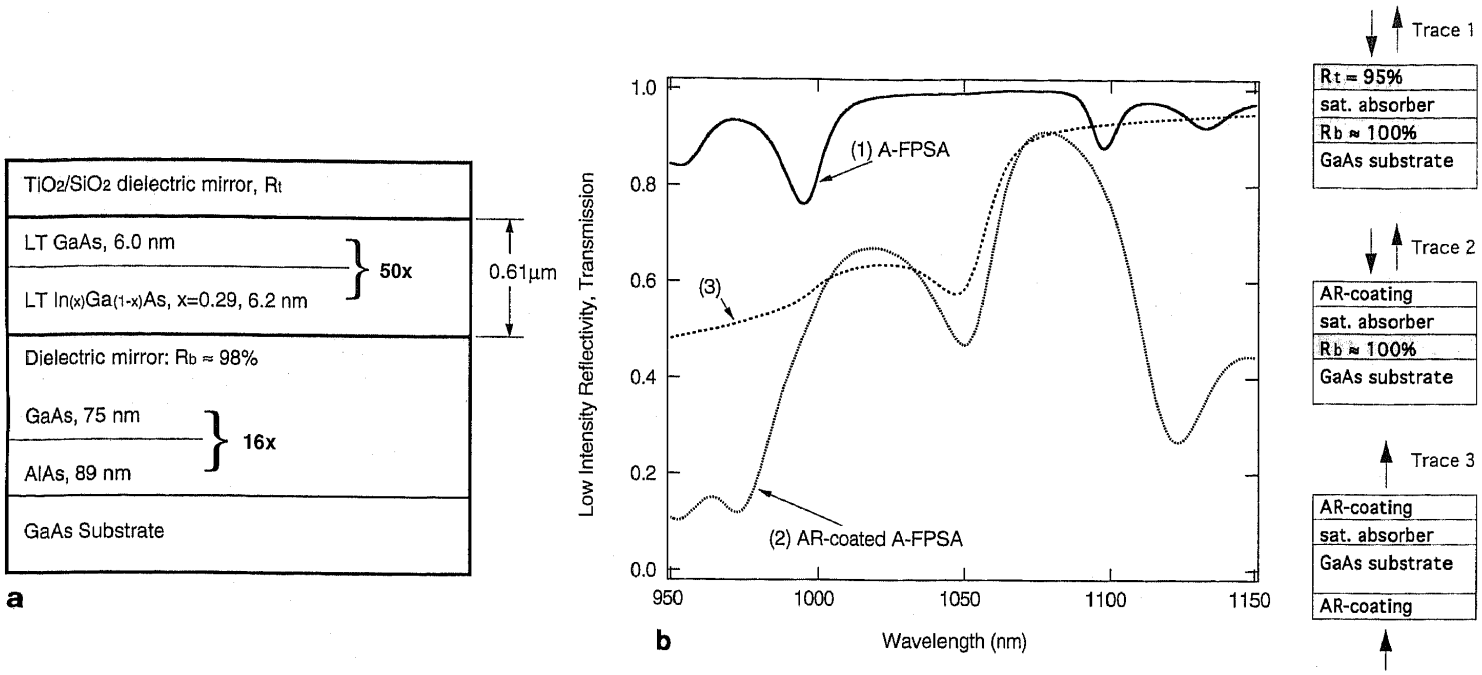

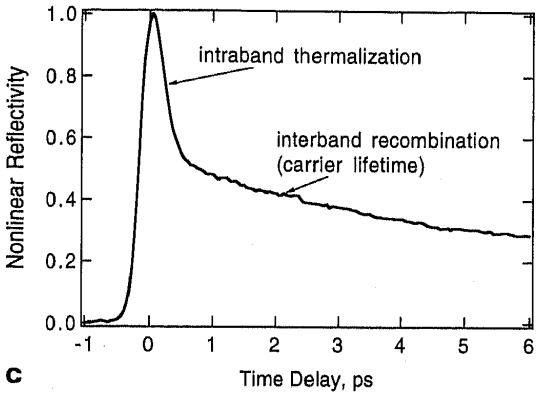

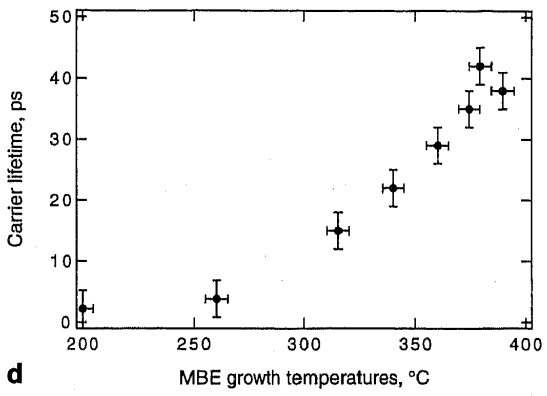

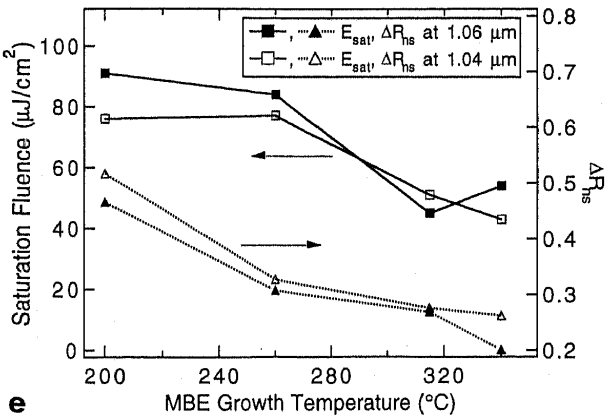

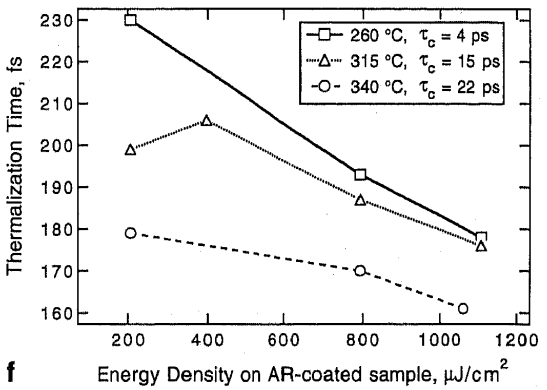

Fig. 4. **a** A–FPSA design cross section for a laser wavelength ≈ 1.05 μm. The top reflector is typically high between 90% to 98%. The thickness of the low-temperature MBE-grown In GaAs/GaAs saturable absorber is chosen for antiresonance operation. The free spectral range is ≈ 100 nm limited by the bottom mirror

b Low-intensity reflectivity measurements of the A–FPSA structure described in **a** grown at $\approx 380°$ C with a carrier lifetime of ≈ 40 ps. Trace 1 shows the reflectivity of the final A–FPSA, trace 2 of the AR-coated A–FPSA, and trace 3 the transmission of an AR-coated reference sample MBE-grown at the same time on a GaAs substrate without the bottom reflector. The exciton wavelength is ≈ 1.05 μm and the resonance dips are due to the final bandwidth of the bottom reflector

c Measured bitemporal impulse response of the A–FPSA using a femtosecond A–FPSA mode-locked Nd:glass laser. The fast component is due to intraband thermalization and the slow component due to carrier recombination

d Carrier lifetime as a function of the MBE-growth temperature. A semiconductor grown at normal temperature ($\approx 600°$ C) has a carrier lifetime in the nanosecond regime

e Measured saturation fluence E_{sat} and the nonsaturable background loss ΔR_{ns} as a function of MBE-growth temperature at a wavelength of 1.06 μm and 1.04 μm. The measurements were done on AR-coated A–FPSA samples to obtain a sufficiently high incident energy density typical for cw mode-locked lasers. The effective saturation fluence for an A–FPSA is then given by $E_{sat,eff} = (1/\xi)E_{sat}$ (11)

f The measured thermalization time constant of the AR-coated A–FPSA samples. The energy density incident on an A–FPSA E_{in} produces an energy density inside the Fabry-Perot structure $E_c = \xi E_{in}$ (11) which is equivalent to the AR-coated incident energy density

Around antiresonance within the high reflectivity band we obtain negligible group-delay dispersion using a sufficiently high top reflector. The low group-delay dispersion can support sub-100 fs pulse durations and is a clear advantage of an antiresonant Fabry-Perot structure with a large free spectral range and a sufficiently high top reflector [50]. The free spectral range has to be larger than the bandwidth of the laser to prevent multiple pulses reflected from the A–FPSA. In contrast, at resonance we observe a strong group-delay dispersion and a group delay that is typically many times longer than the Fabry-Perot round trip period due to the constructive interference of the reflected fields in the Fabry-Perot. For example, the resonance enhancement of the group-delay dispersion has been used by the Gires-Tournois Interferometers (GTI) [51] which is a low-Q non-absorbing Fabry-Perot reflector with a large group-delay dispersion optimized to compensate positive dispersion in short-pulse generation [40].

The nonlinear reflectivity change in the A–FPSA is due to bandfilling where the absorption is bleached with the photo-excited carriers due to the Pauli exclusion principle. The measured impulse response of the A–FPSA shows a bitemporal behavior (Fig. 4c) with a fast component due to intraband thermalization and a slow component due to interband recombination (i.e., carrier recombination). The carrier lifetime in semiconductor materials grown at normal MBE temperatures ($\approx 600°$ C) is in the nanosecond regime, however, at a lower growth temperature it can be reduced continuously (Fig. 4d). We can control the stability and starting mechanisms for the passive mode-locking process directly by changing the dynamic properties of the semiconductor material. For example, by adjusting the carrier recovery time, we can control the pulse build-up time and create a device that causes the laser to either Q-switch or mode-lock without affecting intracavity losses. Generally, a longer carrier lifetime improves self-starting of passive mode locking without affecting intracavity losses but with an upper limit determined by the onset of self-Q-switching.

The passive mode locking starts from mode-beating noise spikes because the laser can more strongly bleach the saturable absorber with pulses. Absorption bleaching can be modeled with a nonlinear absorption coefficient:

$$\alpha_s/(1+x)+\alpha_{ns}, \tag{7}$$

where α_s is the part of the absorption coefficient that can be saturated, α_{ns} is the part that cannot be saturated (such as scattering losses), and x determines the absorption bleaching. In the case of a cw mode-locked laser, the average power does not significantly change between cw and mode-locked operation. For cw lasing, x_{cw} is given by

$$x_{cw} = I/I_{sat}, \tag{8}$$

where I is the average intensity incident onto the saturable absorber, and I_{sat} is the cw saturation intensity given by

$$I_{sat} = h\nu/\sigma_a\tau_c, \tag{9}$$

where $h\nu$ is the photon energy, σ_a is the absorption cross section, and τ_c is the carrier lifetime. The saturable absorber has a carrier lifetime τ_c typically longer than the pulse duration τ_p and much shorter than the pulse repetition period $T \approx 1$ ns to 10 ns. Therefore, under mode-locked operation, the absorption bleaching, and hence the reflectivity, is increased due to the increased numbers of carriers generated within the duration of one laser pulse. For $\tau_p < \tau_c$ (i.e., no significant carrier recombination during the pulse duration), and $T \gg \tau_c$ (i.e., the saturable absorber fully recovers between consecutive pulses), x_p is given by

$$x_p \cong \frac{E_p}{E_{sat}} = \frac{I}{I_{sat}}\frac{T}{\tau_c} = x_{cw}\frac{T}{\tau_c} > x_{cw}, \tag{10}$$

where E_p is the pulse energy density, and $E_{sat} = h\nu/\sigma_a$ is the saturation fluence. Equation (10) expresses that the absorption is more strongly bleached at pulsed than at cw lasing provided that at cw intensities the absorption is not bleached. A stronger bleached absorber increases the reflectivity of the A–FPSA. The nonlinear reflectivity (i.e., difference between cw and mode-locked reflectivity) decreases with increased pulse-repetition rate and increases with a shorter carrier lifetime, as long as $\tau_c > \tau_p$.

The saturation fluence E_{sat} and the non-saturable background losses $\Delta R_{ns} \equiv 1 - R(E \to \infty)$ (Fig. 4e) have been determined from the measured reflectivity as a function of incident pulse energy density on the AR-coated samples using a theoretical fit based on a traveling-wave rate-equation model [50]. For this measurement we chose to increase the pulse duration to ≈ 1.4 ps in order to determine the saturation fluence of the thermalized carrier distribution at a wavelength of 1.06 μm. The cw saturation intensity $I_{sat} = E_{sat}/\tau_c$ (9) follows then directly from the carrier lifetime τ_c. Because the measurements are performed on AR-coated samples the effective saturation fluence of the A–FPSA at antiresonance is increased by a factor of $1/\xi$ [50]:

$$E_{sat,eff} = \frac{1}{\xi}E_{sat}, \text{ with } \xi = \frac{1-R_t}{(1+\sqrt{R_tR_b}e^{-2\alpha d})^2}, \tag{11}$$

where R_t and R_b are the reflectivities of the top and bottom mirror, respectively, and d, n, and α the thickness, refractive index, and amplitude absorption coefficient of the absorber. Thus, it is possible to choose the proper saturation fluence by varying R_t, d, or the absorption edge. We typically used a 95% top reflector which yields a ξ of 0.018, causing an increase of the saturation fluence by a factor of 56. With the measured reflectivity changes of AR-coated A–FPSA samples we can calculate the nonlinear reflectivity change $\Delta R = R_{cw} - R_{pulsed}$ for the final A–FPSA [50]. This nonlinear reflectivity change produces a loss-coefficient reduction Δl given by

$$\Delta l = \Delta R/R \cong \Delta R \text{ for } R \cong 1. \tag{12}$$

Equations (6) and (12) can be used to compare the contributions of KLM and A–FPSA mode locking.

The dominant mode-locking mechanism of the A–FPSA is the nonlinear reflectivity change due to band-

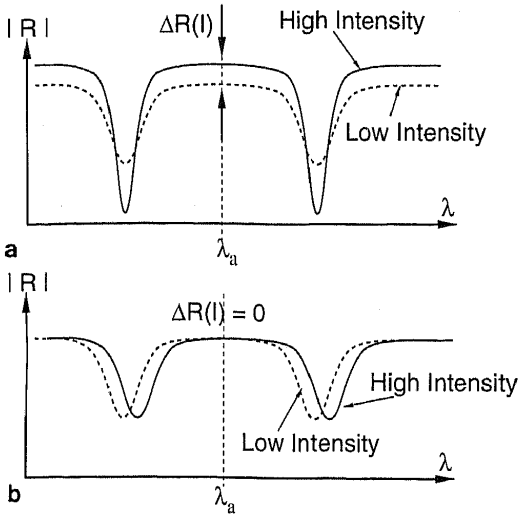

Fig. 5a, b. Nonlinear reflectivity $\Delta R(I)$ of the A–FPSA: (**a**) due to absorption bleaching, and (**b**) due to a reactive nonlinearity such as the free-carrier-induced refractive-index change. A reactive nonlinearity produces only a wavelength shift of the resonance but does not change the reflectivity at antiresonance λ_a as long as the nonlinear shift is much smaller than the free spectral range

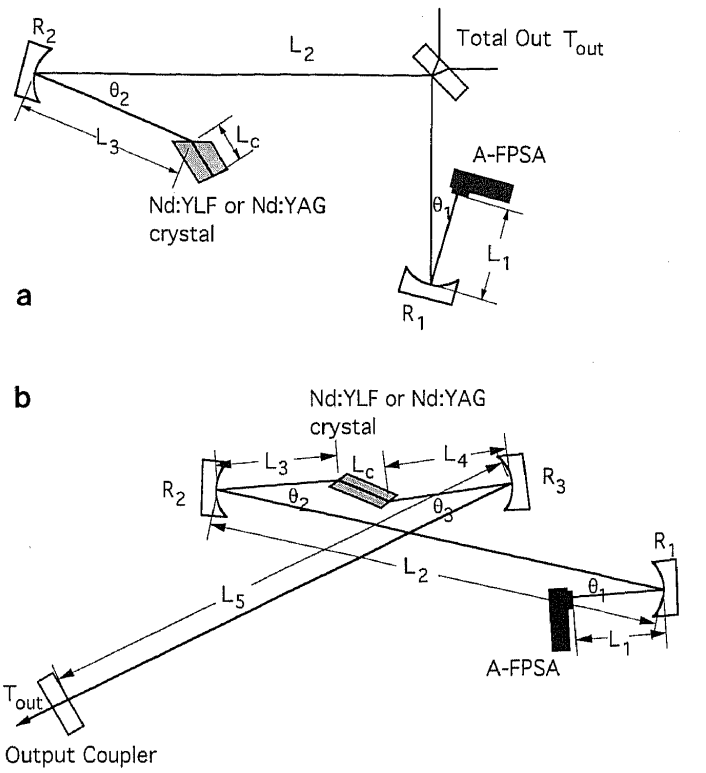

Fig. 6a, b. End-pumped astigmatically compensated linear Nd:YLF or Nd:YAG cavity: **a** Gain-at-End cavity, called GE cavity, **b** Gain-in-Middle cavity, called GM cavity

filling. Reactive nonlinearities inside the A–FPSA such as nonlinear phase shifts due to free carriers, Kerr-effect, etc., do not result in any significant change in reflectivity at antiresonance (Fig. 5). However, such reactive effects form a nonlinear lens that can lead to self-focusing of the cavity mode in the gain medium which results in higher gain similar to KLM. The most significant reactive contribution in the A–FPSA is the refractive-index change due to the photo-generated carriers. However, the self-focusing effect of the A–FPSA is much smaller than the nonlinear reflectivity change due to bandfilling because of the rather thin absorber layer of < 1 μm and because of the antiresonance operation of the Fabry-Perot saturable absorber with an R_t typically above 90% [50].

Even though the non-saturable background losses ΔR_{ns} (Fig. 4e) increase with lower MBE growth temperature, its effect on intracavity losses is strongly reduced for an A–FPSA with a high top reflector. The measured fast component [50] also depends on the MBE-growth temperature (Fig. 4f). The intraband thermalization is faster for samples grown at higher temperature and for higher energy densities. The measurements are done on AR-coated samples, thus for an A–FPSA device the energy density E seen by the saturable absorber corresponds to the energy density used in Fig. 4f and is a factor ξ (11) smaller than the incident energy density E_{in} (i.e., $E = \xi E_{in}$).

4 Picosecond Mode-Locking Regime

The bitemporal impulse response of the A–FPSA (Fig. 4c) provides efficient self-starting due to the longer carrier lifetime but also supports pulse durations shorter than the carrier lifetime due to the fast sub-picosecond component [2]. The obtained pulse duration is predominantly limited by the gain bandwidth of picosecond lasers such as Nd:YLF and Nd:YAG. We did not use any GVD compensation in the picosecond regime. Generally, strong nonlinearities and low intracavity losses minimize pulse durations.

The main challenge in passive cw mode locking of Nd:YLF and Nd:YAG is the suppression of self-Q-switching instabilities which are enhanced with a long upper-state lifetime [52]. The main advantage of the A–FPSA is that the parameters such as saturation intensity and loss can be adjusted as required. We have demonstrated that the A–FPSA, used as a compact nonlinear end-mirror in a cw-pumped linear cavity (Fig. 6), starts and sustains passive mode locking without self-Q-switching [1, 2, 3].

Other self-starting passive mode-locking techniques have been unable to suppress self-Q-switching instabilities [53, 54]. KLM is very weak in the picosecond regime (see detailed discussion in Sect. 6), and needs a starting mechanism such as an acousto-optic mode-locker [55, 56]. Under certain conditions, once mode locking is started, the acousto-optic mode-locker can be turned off without affecting the pulse train. A KLM-diode-pumped Nd:YLF laser with the gain medium at the end of the linear cavity produced pulse durations of 6 ps, but to enchance KLM, an additional Kerr medium such as a 1 cm Brewster-angled rod of SF57 was placed at an intracavity focus of ≈ 30 μm [55]. A KLM-Nd:YAG laser produced 8.5 ps pulse duration [56]. In comparison, actively mode-locked diode-pumped Nd:YLF lasers [57–59] using an acousto-optic modulator produce pulses as short as 7 ps [58], and a diode-pumped Nd:BEL laser produced pulses as short as 2.9 ps [60]. These results were

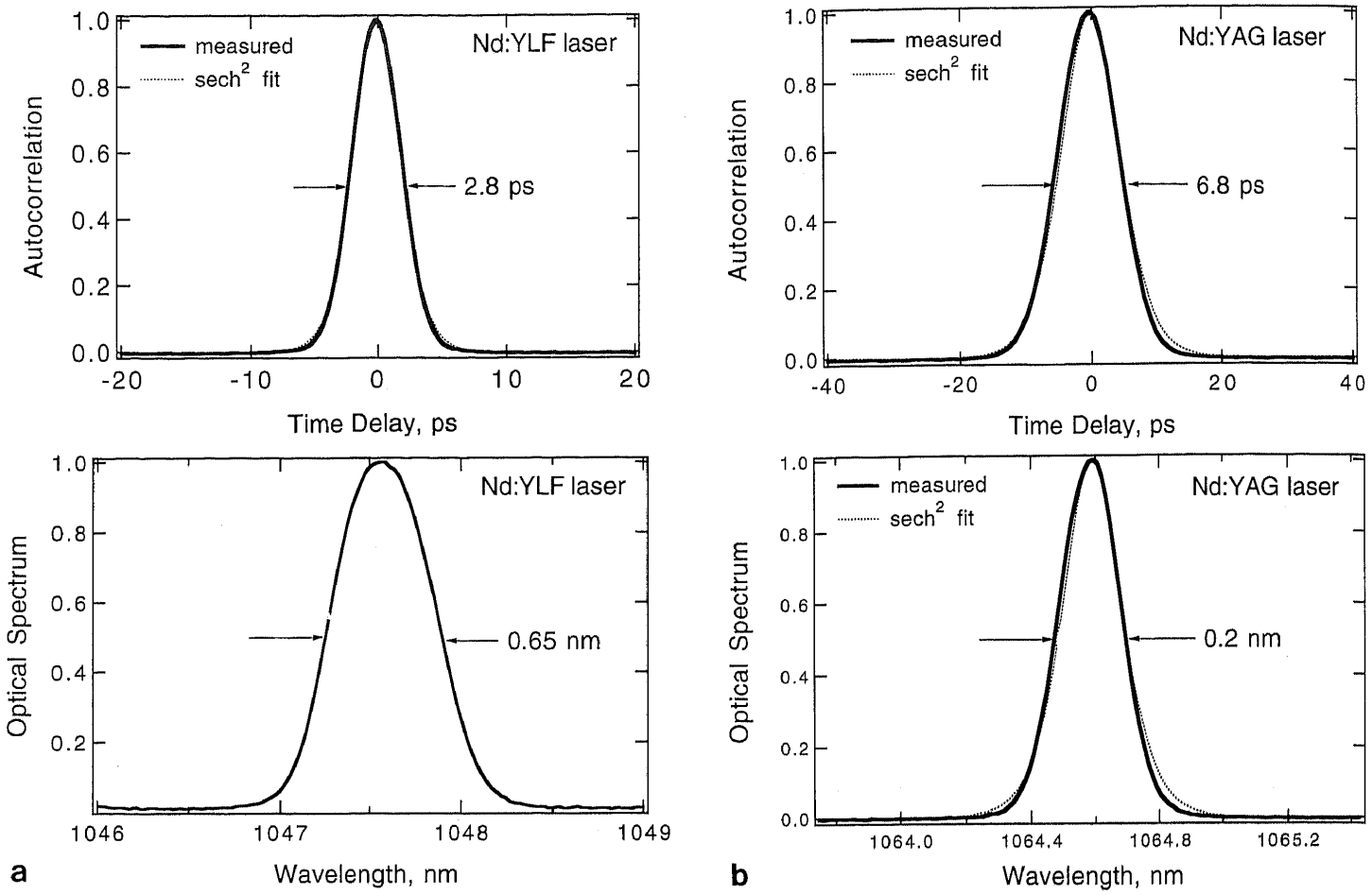

Fig. 7. **a** A–FPSA mode-locked Nd:YLF laser: GE cavity with $R_1 = 10$ cm (Fig. 6a), 220 MHz pulse-repetition rate, 1.5% output coupler, A–FPSA with $R_t = 95\%$ and 22 ps carrier lifetime, average output power of 460 mW (both beams), time-bandwidth product ≈ 0.5. **b** A–FPSA mode-locked Nd:YAG laser: GE cavity with $R_1 = 10$ cm (Fig. 6a), 217 MHz pulse-repetition rate, 1.5% output coupler, A–FPSA with $R_t = 91\%$ and 22 ps carrier lifetime, average output power of 400 mW (both beams), time-bandwidth product ≈ 0.38

achieved in the middle of the stability regime where KLM is negligible. Therefore, the combination of KLM and an acousto-optic modulator as a starting mechanism does not bring a big advantage over simple active mode locking in the picosecond regime. However, a simple passive technique alone, such as an A–FPSA, reduces the complexity of mode-locked picosecond solid-state lasers which have the potential to produce more than 1 W average power at high repetition rates.

We have investigated two types of cavity designs (Fig. 6). In one case, the gain medium is placed at the end of the linear laser cavity, referred to by "Gain-at-End" (GE) cavity (Fig. 6a). In the other case, the gain medium is placed approximately in the middle of the laser cavity, referred to by "Gain-in-Middle" (GM) cavity. Using an A–FPSA for passive mode locking, the GE cavity achieved pulses as short as 2.8 ps for Nd:YLF (Fig. 7a) and 6.9 ps for Nd:YAG (Fig. 7b), while the GM cavity had pulses only as short as ≈ 10 ps for Nd:YLF. Broader pulses are also expected for the GM Nd:YAG cavity. For the GE cavity, the mode-locked time-bandwidth product is typically ≈ 1.5 to 2.2 times above the ideal product for a sech^2 pulse shape due to enhanced Spatial Hole Burning (SHB) [61]. In contrast, the GM cavity has nearly ideal time-bandwidth limited performance. The extension to diode pumping was demonstrated with both a Nd:YLF and a Nd:YAG laser producing pulse durations as short as 5.1 ps and 8.3 ps, respectively [3].

Independent of the mode-locking mechanism the effects of SHB significantly reduce the pulse width in end-pumped lasers when the gain region is at one end of the laser cavity and when its length is on the order of the pulse length (Fig. 6a, GE-cavity) [61]. This occurs because the frequency separation between modes that fill the available spatial holes increases as the gain region is moved from the middle of the cavity to the end of the cavity. This results in an increase of the effective inhomogeneously-broadened line width which allows for shorter pulse generation and shorter mode-locking build-up time for both active mode locking and A–FPSA mode locking [61]. Because of the extra axial modes already running cw in the GE cavity, the mode-locker or the saturable absorber only needs to fill in the missing modes between the available running modes until they overlap and phase-lock together. With the GM cavity however, the mode-locker or the saturable absorber must force energy from one or two axial modes at line center into all of the other modes. The effects of SHB persist even in steady state for the GE cavity because the pulse over-

laps itself at the end mirror, allowing for SHB within the gain region, whereas the GM cavity has no SHB when running mode-locked at steady state. It is interesting to note that for KLM lasers SHB in a GM cavity can be responsible for self-starting difficulties [36, 62]. For example, self-starting KLM was demonstrated with a ring cavity [36]. In contrast, we observed a reduced mode-locking build-up time with enhanced SHB in a GE-cavity.

The top reflector of the A–FPSA is a critical parameter for stable modelocking. Therefore, special care was taken to measure the absolute reflectivity of the top coating using the "VW-technique" of a Varian Cary 5E spectrophotometer. In addition, we confirmed this measurements with insertion loss measurements in a Nd:YLF laser. Using the more accurate VW-technique we measured slightly lower top reflectivities than previously reported [1–3, 5]. For the Nd:YLF laser we obtained stable modelocking without self-Q-switching with an A–FPSA using an R_t of 95%. Self-Q-switching could not be prevented for an R_t of 91%. For the Nd:YAG laser self-Q-switching was suppressed for both top reflectors due to the lower upper-state lifetime of Nd:YAG (Table 1). The larger nonlinearity obtained with a lower top reflector can overcome the expected pulse increase with higher intracavity losses [63] (Fig. 12) and still produce shorter pulses. For example with a Nd:YAG laser we routinely obtained ≈ 10 ps pulse durations with a 95% top reflector (i.e., unbleached insertion loss of $\leq 1\%$) and ≈ 7 ps pulse durations with a 91% top reflector (i.e., unbleached insertion loss of $\leq 2\%$). The lower small-signal gain in diode-pumped lasers typically required a higher top reflector to prevent self-Q-switching [3]. The Self-Q-switching operation will be further discussed in Sect. 7.

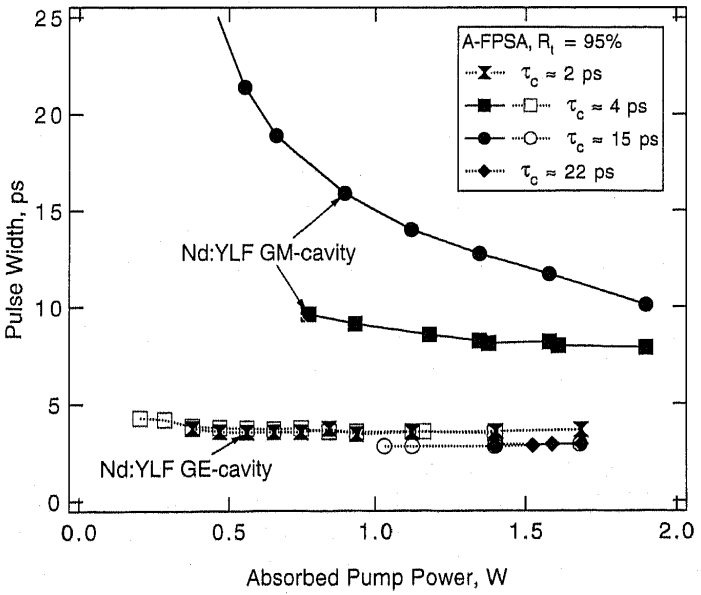

Fig. 8. A–FPSA mode-locked Nd:YLF laser in the GE- and GM-cavity configuration. Enhanced Spatial Hole Burning (SHB) of the GE cavity produces shorter but not time-bandwidth transform-limited pulses. For a GM cavity the pulse duration shows a stronger carrier-lifetime dependence and is typically longer but time-bandwidth transform-limited

The final pulse duration shows an interesting dependence on the carrier lifetime. In the case of a GE Nd:YLF cavity we obtain significantly shorter pulse durations than the carrier lifetime of the A–FPSA and the final pulse duration does not strongly depend on the carrier lifetime (Figs. 8, 12). Even in the case of a less inhomogeneously broadened gain, such as in a GM Nd:YLF cavity, we obtained pulse durations shorter than the response time of the saturable absorber, i.e., the carrier life time (Figs. 8, 12). However, we observe a stronger dependence on the carrier lifetime with, surprisingly, a shorter pulse duration with a longer carrier lifetime. The results shown in Fig. 8 cannot be explained by current existing theories for fast absorber mode locking [63, 64] which requires a saturable-absorber recovery time, i.e., a carrier lifetime, much shorter than the pulse duration. Consequently, the mode-locking theory without any dynamic gain saturation, such as the fast absorber mode-locking theory, needs to be extended for a bitemporal saturable absorber and inhomogeneous broadening.

5 Self-Starting Dynamics of A–FPSA Mode-Locking

The semiconductor A–FPSA has a bitemporal absorption response. The slow component provides the self-starting mechanism [2] and without significant Kerr-lens contribution the fast component is necessary to support further pulse shortening [5]. The carrier lifetime of the bitemporal A–FPSA (Fig. 4a) was varied by the MBE-growth temperature to characterize its influence on the self-starting and self-Q-switching dynamics of a cw mode-locked Nd:YLF. The absorption at 1.047 μm is approximately the same for all samples (Fig. 9). The small variations in the reflectivity for the AR-coated samples have only a negligible effect on the final A–FPSA with a top reflector of 95%. All samples produced an unbleached insertion loss of $1.0\% \pm 0.1\%$. Because small variations of

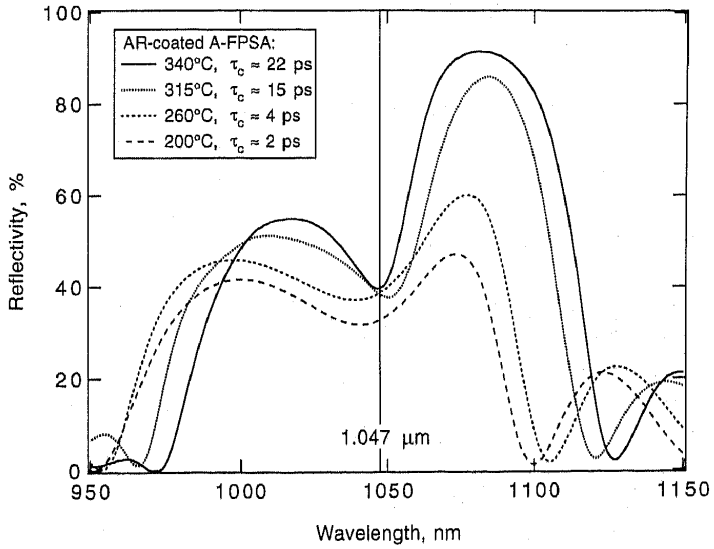

Fig. 9. Low-intensity reflectivity of AR-coated A–FPSA samples grown at different MBE-growth temperatures

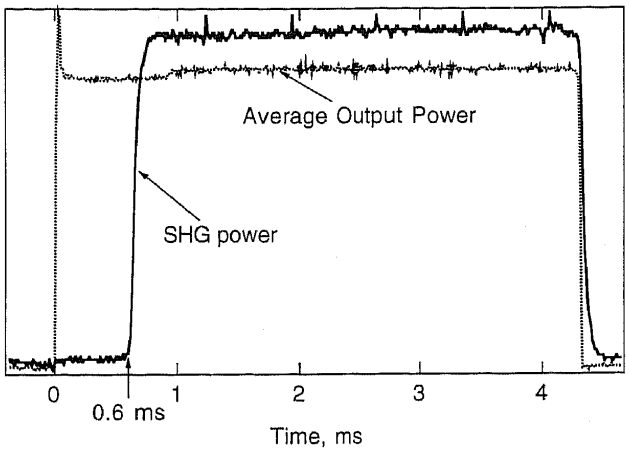

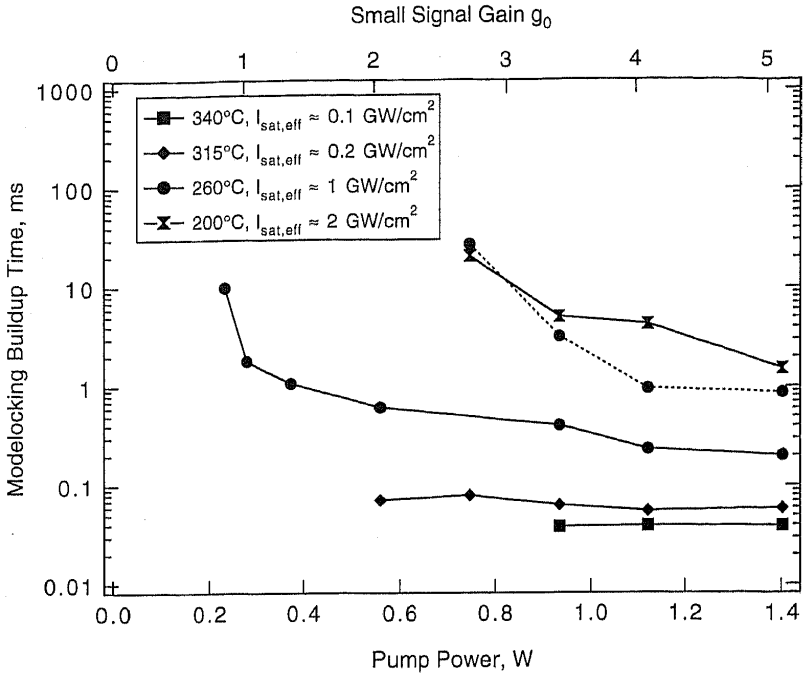

Fig. 10a, b. A–FPSA mode locking is self-starting. **a** The mode-locking build-up time is determined with an intracavity chopper monitoring both the average output power and the average power of the Second-Harmonic Generated signal (SHG). The SHG signal is proportional to the peak intensity squared and therefore strongly pulse-width dependent. The delay in the SHG signal determines the mode-locking build-up time. **b** Mode-locking build-up time for an A–FPSA mode-locked GE-cavity Nd:YLF laser. A smaller $I_{sat,eff}$ produces a stronger mode-locking driving force. In comparison, a GM cavity typically requires a slightly longer mode-locking build-up time.

the top reflector have, however, a strong influence on the final nonlinearity, we coated all of the A–FPSA samples at the same time with the same coating run.

The mode-locking build-up time was measured with a GE-cavity Nd:YLF laser operated in the middle of the cavity stability regime as described before [1]. The slope efficiency for a 1.5% output coupler was 35% (both output beams) and the pump threshold was ≈40 mW. We used an intracavity mechanical chopper to study the self-starting dynamics and monitor both the average power and the Second-Harmonic Generation (SHG) signal of the Nd:YLF laser. The transient starting behavior of a Nd:YLF laser is shown in Fig. 10a, at 0.37 W cw pump power using the A–FPSA grown at 260° C and a 1.5% output coupler. After ≈600 μs delay the SHG signal sharply increases and indicates that short pulses have formed because the second-harmonic signal increases inversely proportional to the pulse duration assuming constant pulse energy. Therefore, the delay of the second-harmonic signal determines the mode-locking build-up time. At this low pump power the average build-up time is 1.1 ms with a standard deviation of 0.5 ms. At higher pump powers the standard deviation becomes much smaller. The average buildup time of a stable cw mode-locked Nd:YLF laser (no self-Q-switching) is summarized in Fig. 10b. A mode-locking build-up time of ≈1 ms corresponds to ≈200000 cavity round trips. Both the laser mode inside the gain medium and on the saturable absorber are kept constant for each A–FPSA sample. No other cavity parameters were altered while changing from one A–FPSA sample to the others, because the output power was peaked up by adjusting the alignment of the A–FPSA mirror alone and by maintaining the same pulse-repetition rate. In comparison, similar measurements determined a 200 μs build-up time for passively mode-locked Ti:Sapphire lasers [65, 66] and a 15 μs build-up time for a CPM dye laser [67].

Because E_{sat} (Fig. 4e) and $E_{sat,eff}$ (11) do not vary drastically with the growth temperature above the absorption edge, $I_{sat,eff}$ basically scales inversely with the carrier lifetime (7). Thus, a longer carrier lifetime produces a smaller $I_{sat,eff}$, therefore a shorter mode-locking build-up time (Fig. 10b). Heating of the A–FPSA samples due to nonradiative relaxation processes will red-shift the absorption edge and therefore slightly increase the effective saturation intensities. The larger nonsaturable background losses ΔR_{ns} (Fig. 4e) at lower growth temperature will further decrease the nonlinear reflectivity change but because of the high top reflector it has no significant effect. A more detailed characterization of the A–FPSA samples is given in [50].

A shorter mode-locking build-up time is obtained with a longer carrier lifetime or a smaller $I_{sat,eff}$. However, for a given top reflector the upper limit of the carrier lifetime is set by the onset of self-Q-switching [2]. As expected, the mode-locking build-up time becomes longer with a lower small-signal gain (Fig. 10b) and a larger output coupler corresponding to a smaller photon cavity lifetime. The small-signal gain was determined with relaxation frequency measurements [68]. In addition, we also measured a shorter mode-locking build-up time with a Nd:YAG laser which has a larger gain cross section (Table 1) and therefore a larger small-signal gain.

From the measured nonlinear reflectivity change, we can calculate for the A–FPSA samples a mode-locking driving force $d(\Delta R)/dI$ with $I->0$ which is inversely proportional to $I_{sat,eff}$ [50]. For our samples with a 95% top reflector at a wavelength of 1.047 μm, the mode-locking driving force $d(\Delta R)/dI$ with $I->0$ is approximately 0.4×10^{-11} cm²/W, 2.3×10^{-11} cm²/W, and 4.4×10^{-11} cm²/W for the A–FPSA samples with $R_t=95\%$ and an MBE-growth temperature of 260° C, 315° C, and 340° C, respectively [50]. As expected, a larger mode-locking driving force reduces the mode-locking build-up time (Fig. 10b). In comparison, the analogous mode-locking driving force $d(\Delta g)/dI$ with $I->0$ for KLM is $\approx10^{-13}$ cm²/W (see Sec. 6). The KLM driving force in comparison to the A–FPSA mode-locking driving force is even more reduced because the mode size in the laser crystal is typically more than 10 times larger than the focused mode on the A–FPSA.

6 Representative Example: Passively Mode-Locked Nd:YAG Laser

As a representative example we discuss a Ti:Sapphire-Laser-Pumped Nd:YAG laser in more detail. Similar results, however, were achieved with a Nd:YLF laser and with diode-laser pumping. In this section we present a detailed quantitative discussion of A–FPSA mode locking and set it in comparison to KLM.

The parameters of the GE Nd:YAG cavity are (Fig. 6a): A–FPSA with an $R_t\approx95\%$ (Figs. 4a, b), carrier lifetime ≈40 ps. The cavity parameters are given by $\theta_1=8°$, $L_2=53$ cm, $\theta_2=10°$, $R_2=20$ cm, $L_3=9.9$ cm, $L_c=4$ mm. To vary the spot size on the A–FPSA we chose in one case $R_1=10$ cm, $L_1=5.3$ cm giving a pulse-repetition rate of 218 MHz, and in the other case $R_1=5$ cm, $L_1=2.56$ cm giving a pulse-repetition rate of 227 MHz. In both cases L_1 is adjusted for the middle of the cavity stability regime which was confirmed experimentally by moving the A–FPSA sample in both directions until it stopped lasing. The calculated beam radius using ABCD matrix formalism are shown in Fig. 11.

The Nd:YAG crystal is on one side cut at Brewster's angle and on the other side cut flat with an AR-coating for the pump wavelength of 808 nm and an HR-coating for the lasing wavelength 1.06 μm. The Nd:YAG laser is pumped with a cw Ti:Sapphire laser at a wavelength of 808 nm and a measured pump radius of 20 μm. 74% of the incident pump power is absorbed in the Nd:YAG crystal. The slope efficiency with respect to the absorbed pump power (both output beams) for $T_{out}=1.5\%$ is 43% with a pump threshold of ≈20 mW and for $T_{out}=2.8\%$ is 50% with a pump threshold of ≈25 mW. The low-intensity unbleached insertion loss of the A–FPSA sample is $\approx1\%$, which is reduced by $<0.5\%$ when the laser is mode-locked.

Figure 12 shows the pulse width as a function of pump power or intracavity average power for both cavities and two different output couplers T_{out}. The mode locking is always self-starting and the threshold for pulse formation depends on the incident energy density on the A–FPSA (Fig. 12). Therefore, for the extension to high-power

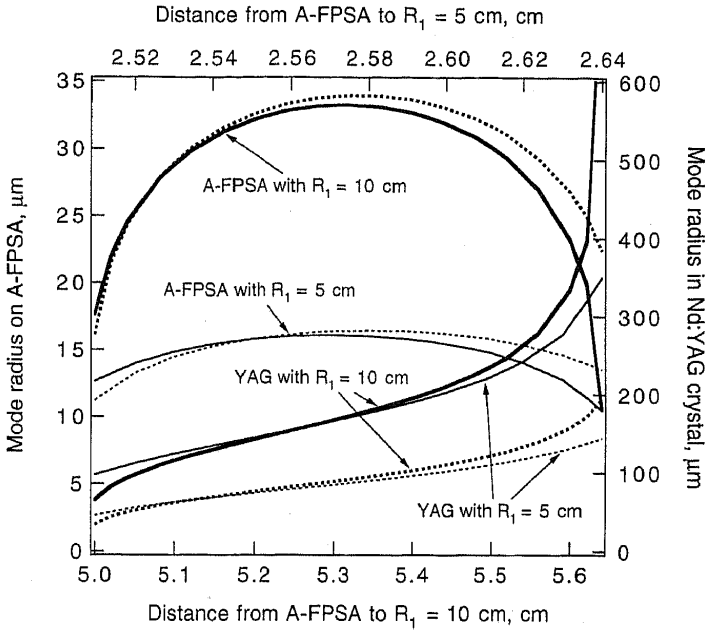

Fig. 11. GE-cavity Nd:YAG laser. Calculated mode sizes on the A–FPSA mirror and inside the Nd:YAG crystal over the cavity stability regime modified by L_1 which is the distance form A–FPSA to R_1 (Fig. 6a). The mode radius is calculated for both the sagital *(dashed lines)* and the tangential *(solid lines)* planes. For a smaller mode size on the A–FPSA using $R_1=5$ cm *(fat lines)* we observe a stability range for $L_1\approx2.51$ cm to 2.65 cm. For a larger mode size on the A–FPSA using $R_1=10$ cm *(thin lines)* we observe a stability range for $L_1\approx5$ cm to 5.7 cm

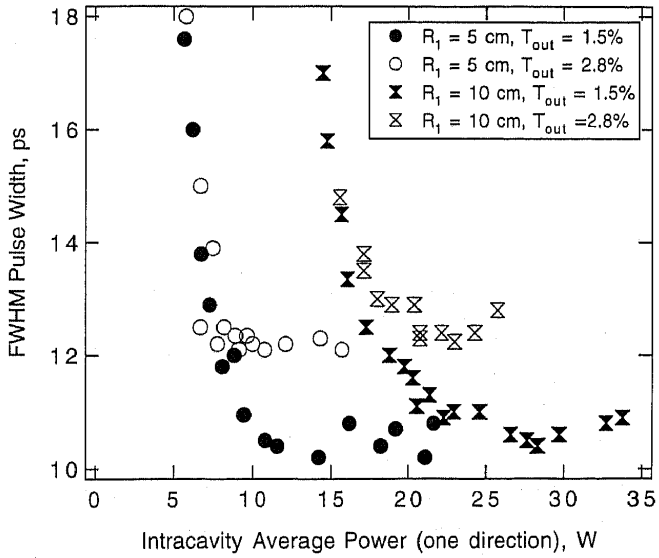

Fig. 12. GE-cavity Nd:YAG laser. Pulse duration as a function of pump power, laser mode size on A–FPSA, and different output couplers. The mode locking is always self-starting using an A–FPSA with $R_t=95\%$, and a carrier lifetime of 40 ps

lasers the mode area on the A–FPSA mirror can be increased to prevent damage without degrading self-starting und mode locking. With a smaller spot size of 8.1×10^{-6} cm² on the A–FPSA using $R_1=5$ cm, the mode-locking starts at ≈6 W average intracavity power or at ≈3.3 mJ/cm² pulse-energy density. Increasing the spot size to 3.5×10^{-5} cm² using $R_1=10$ cm increases the pulse formation threshold to ≈14 W average intracavity power with ≈2 mJ/cm² pulse-energy density. The slight-

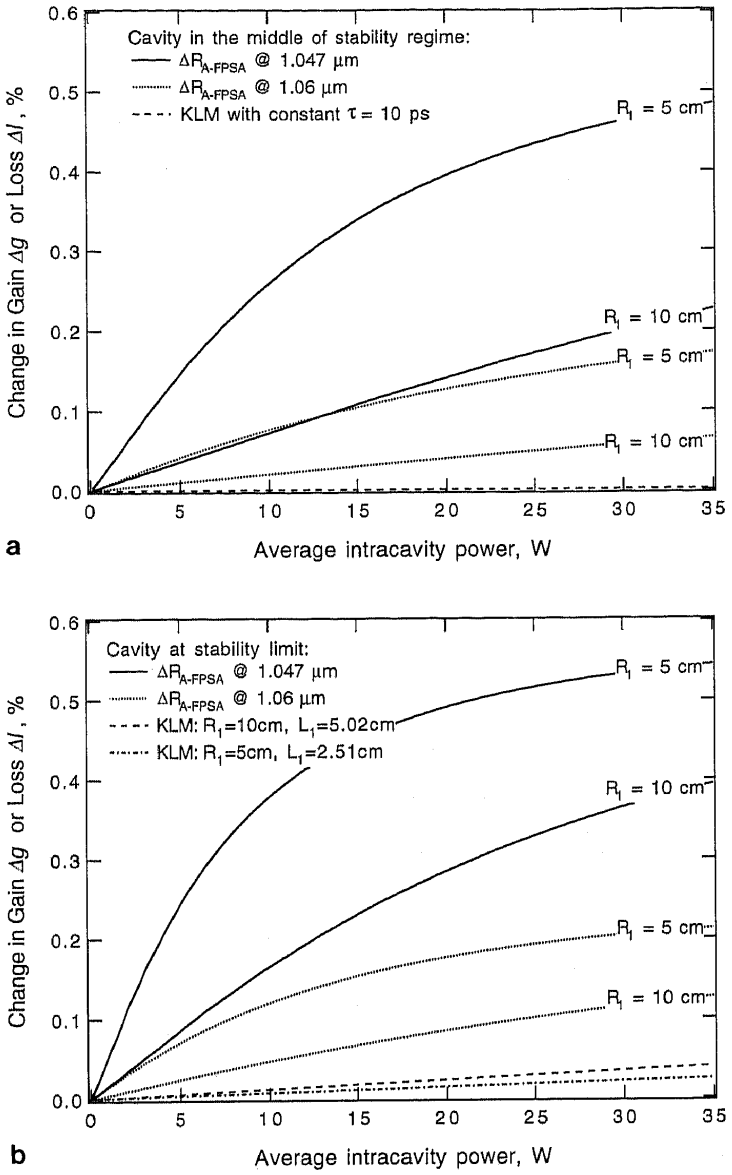

Fig. 13a, b. GE-cavity Nd:YAG laser. Change in gain Δg (6) and loss of the A–FPSA Δl (12), where the A–FPSA has an $R_t = 95\%$, and a carrier lifetime of 40 ps. **a** Cavity in the middle of stability regime with $L_1 = 2.56$ cm for $R_1 = 5$ cm, and $L_1 = 5.3$ cm for $R_1 = 10$ cm. **b** Cavity at the stability limit with $L_1 = 2.51$ cm for $R_1 = 5$ cm, and $L_1 = 5.02$ cm for $R_1 = 10$ cm

ly lower pulse-energy density for the onset of mode-locking can be explained with the higher small-signal gain at higher pump power, which produces a shorter mode-locking build-up time (Fig. 10b).

The pulse width decreases with higher intracavity power because of the larger nonlinear reflectivity change in the A–FPSA (Fig. 13). The final pulse duration is limited by the gain bandwidth of the Nd:YAG laser and the total intracavity losses. Haus's fast saturable absorber theory [63] predicts that with increased intracavity losses the pulse duration increases. Indeed, we observed that the steady-state pulse duration is 10.5 ± 0.2 ps with a 1.5% output coupler and 12.3 ± 0.2 ps for a 2.8% output coupler (Fig. 12). An intracavity loss of $\approx 2\%$ without the output coupler would predict the observed increase in pulse duration assuming that the steady-state pulse duration is proportional to $\sqrt{l}$ ([63], eq. A6). Without the A–FPSA we typically determined an intracavity loss of $\approx 1\%$ without the output coupler. This result confirms how important it is to minimize intracavity losses to not only obtain high output power but also short pulses.

To estimate the contribution of KLM we can calculate the gain increase Δg due to "gain aperturing" (6) alone because there is no hard aperture present inside the laser cavity. The ABCD matrix calculations are very simple because the mode radius, the mode change due to self-focusing, and the pump-beam radius is approximately constant along the Nd:YAG crystal. Therefore, we can use a simple astigmatic Gaussian duct [20, 69] to model self-focusing:

$$\begin{pmatrix} \cos \tilde{\gamma}_i L_c & (n_0 \tilde{\gamma}_i)^{-1} \sin \tilde{\gamma}_i L_c \\ -n_0 \tilde{\gamma}_i \sin \tilde{\gamma}_i L_c & \cos \tilde{\gamma}_i L_c \end{pmatrix}. \tag{13}$$

A parabolic approximation was made for the radial dependence of the refractive index given by $n(r) = n_0 - \tilde{n}_2 r^2/2$. L_c is the crystal length, $n_0 = 1.82$ the refractive index of Nd:YAG, and $\tilde{\gamma}_i$ is given by

$$\tilde{\gamma}_i = \sqrt{\tilde{n}_{2i}/n_0} \text{ with } \tilde{n}_{2i} = 4\,\Delta n_{max}/w^2, \tag{14}$$

where w_i is the mode radius either in the tangential or in the sagital plane, and $\Delta n_{max} = \gamma I_{peak}$ with I_{peak} the peak intensity, $\gamma = 6.2 \times 10^{-16}$ cm^2/W for Nd:YAG [70]. Note, that only at cw we obtain an increase of the Kerr effect by a factor of 2 due to the standing wave in a linear cavity. The matrix (13) determines with ABCD matrix calculations the nonlinear radius changes due to self-focusing and with (6) the gain increase, assuming a constant 10 ps pulse duration, an l of 4.8% (for the larger 2.8% output coupler), and a pump radius of 20 μm. The assumption of a constant pulse duration with increased intracavity power is clearly an upper limit for the contribution of KLM (Fig. 13).

In comparison, (12) determines the loss reduction of the A–FPSA between cw and pulsed oscillations [50] (Fig. 13). In the measurements of E_{sat} we used a low duty cycle acousto-optic modulator to prevent any heating effects. At low intensities the lasing wavelength of 1.06 μm is right at the absorption edge (Fig. 4b). Heating produces a continuous red shift of the absorption edge with increasing intensity so that the exciton peak wavelength is ≥ 1.06 μm for incident intensities of $\geq 2 \times 10^5$ W/cm^2 which corresponds to an intracavity average power of ≥ 8 W for $R_1 = 10$ cm and ≥ 2 W for $R_1 = 5$ cm. Therefore, the measured nonlinear reflectivity change at 1.047 μm is more appropriate for our samples because the measurements of ΔR were done without any heating effects.

In the middle of the cavity stability regime, KLM is much weaker than the nonlinear loss reduction from the A–FPSA (Fig. 13a). At an average intracavity power of 35 W we determined a nonlinear gain increase Δg of only 0.0006%. At the stability limit with a longer L_1 we calculate a mode increase due to self-focusing which actually produces a gain reduction and therefore does not lead to saturable absorber action. However, for a shorter L_1, close to the stability limit, we obtain a larger KLM

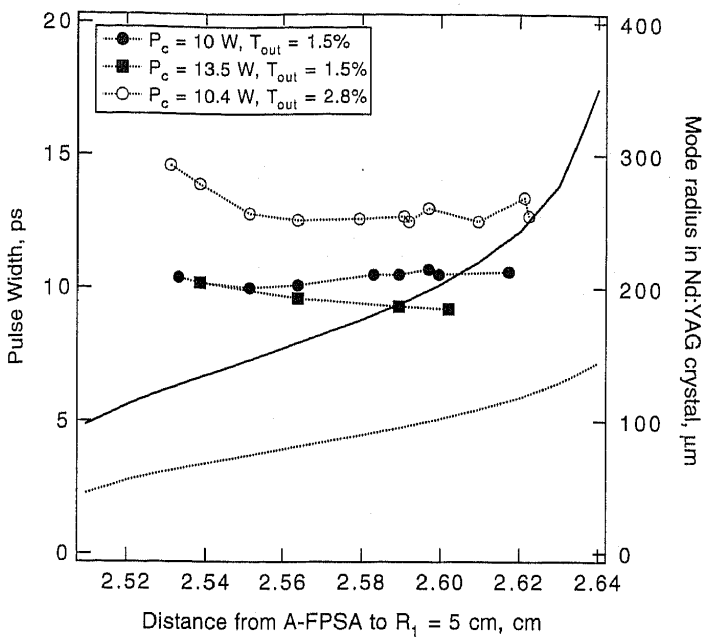

Fig. 14. GE-cavity Nd:YAG laser with $R_1 = 5$ cm. Pulse duration as a function of L_1 which is the distance from the A–FPSA to R_1 (Fig. 6a). KLM does not affect the final pulse duration which is further confirmed by an approximately constant pulse duration as a function of L_1: For $L_1 \leq 2.56$ cm self-focusing produces a fast saturable absorber with $\Delta g > 0$ because $A_{l,\text{pulsed}} < A_{l,\text{cw}}$ (6). For $L_1 \geq 2.56$ cm self-focusing actually prevents any saturable absorber action because $A_{l,\text{pulsed}} > A_{l,\text{cw}}$, thus $\Delta g < 0$

contribution of $\Delta g \leq 0.03\%$ at $P_c = 35$ W, which is, however, still much weaker than the A–FPSA contribution (Fig. 13b).

In our simple case the KLM driving force $d(\Delta g)/dI$ with $I -> 0$ or $d(\Delta g)/dP_c$ with $P_c -> 0$ follows directly from (6) and the ABCD matrix calculations, where I is the intracavity intensity and P_c the intracavity average power. The latter one is more important for comparison because of the strongly different mode sizes on the A–FPSA and in the Nd:YAG crystal (Fig. 11). The mode-locking driving force for KLM $d(\Delta g)/dP_c$ in the middle of the cavity stability regime is $\approx 8 \times 10^{-10}\ \text{W}^{-1}$ and close to the stability limit $\approx 3 \times 10^{-8}\ \text{W}^{-1}$. In comparison, the mode-locking driving force for the A–FPSA is $\approx 10^{-5}\ \text{W}^{-1}$ for $R_1 = 5$ cm and $\approx 10^{-6}\ \text{W}^{-1}$ for $R_1 = 10$ cm [50].

Besides the negligible mode-locking starting force, KLM also does not contribute to the final pulse formation. This was confirmed with pulse-width measurements as a function of L_1 (Fig. 14). The final pulse duration does not shorten the pulse with stronger KLM (i.e., smaller L_1) and also does not broaden the pulse with "negative KLM" (i.e., longer L_1).

The above given discussion is representative for other picosecond lasers such as Nd:YLF which actually has a smaller Kerr nonlinearity than Nd:YAG, i.e., $\gamma = 1.43 \times 10^{-16}\ \text{cm}^2/\text{W}$ [71]. The contribution of KLM is even more reduced for diode-pumped solid-state lasers where the mode area in the laser crystal is typically larger than discussed above [3].

7 Self-Q-Switching

Self-Q-switching means that the stable mode-locked pulse train at the repetition rate of the cavity round-trip time is strongly amplitude modulated producing stable Q-switched macropulses typically of µs duration at repetition rates close to the relaxation oscillations. For example, a semiconductor saturable absorber such as an InGaAsP film passively Q-switched a Nd:YAG laser [53], and a GaAs wafer passively mode-locked and Q-switched a Nd:YAG laser [54]. Using solid-state saturable dye films also self-Q-switched Nd:glass lasers [72]. For solid-state lasers with shorter upper-state lifetimes self-Q-switching is less of an issue. But even if self-Q-switching can be prevented, semiconductor saturable absorbers still introduce too much loss or tend to be bleached at cw intensities, which results in much lower available output power. For example, an intracavity AR-coated proton-implanted GaAs/AlGaAs saturable absorber was used to passively mode-lock a Cr:LiSAF laser, but the available output power was reduced to 5 mW for 480 mW of absorbed pump power from a Ti: Sapphire laser [73].

In addition, stable mode-locked Q-switched operation can be achieved with the A–FPSA. Figure 15 shows a typical Q-switched pulse train. Each macro pulse contains a train of mode-locked pulses. The exact pulse-repetition frequency can be numerically calculated from the rate equations, but typically has as a perturbation to passive mode locking approximately the same value as the small-signal relaxation oscillation frequency. The condition for Q-switching alone is given by [52]

$$\left|\frac{d(\Delta R)}{dP_c}\right| P_c > \frac{g_0}{g}\frac{T_r}{\tau_2}, \tag{15}$$

where ΔR is the saturated reflectivity change of the A–FPSA within one roundtrip, P_c is the average intracavity power, g_0 is the unsaturated gain coefficient g is the saturated gain which is equal to the total losses l, T_r is the round-trip time of the laser, and τ_2 is the laser's

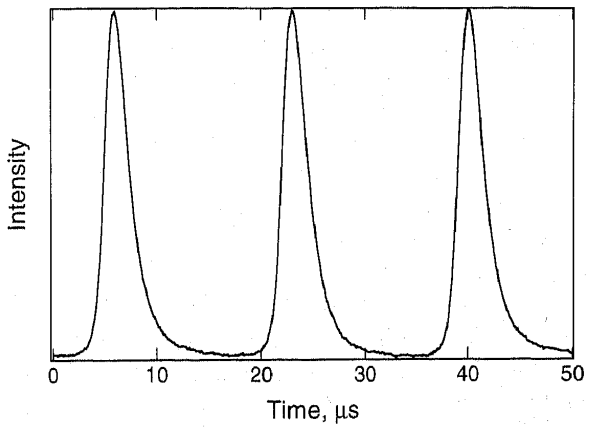

Fig. 15. Self-Q-switched Nd:YLF laser. Q-switched macro pulses typically a few µs long at the repetition rate approximately given by the small-signal relaxation oscillation frequency. The macro pulses are envelope pulses superposed on the cw mode-locked pulse train (not shown) with a pulse repetition rate given by the cavity round-trip time

upper-state lifetime. This equation is essentially comparing the reduction in the loss per round trip from the absorber (left-hand side) to the amount that the gain saturates per round trip (right-hand side). When the differential decrease of loss due to the absorber is larger than the decrease in the saturated gain, the intensity increases each round trip, driving the laser into Q-switched macro pulses (Fig. 15). For a given laser material and A–FPSA parameters, there exists, typically, a range of pump powers between cw and cw mode-locked where stable Q-switching and simultaneous mode-locking is observed.

Equation (15) qualitatively confirms our experimental observations that stable cw mode-locked performance without Q-switching is obtained by pumping the laser harder (i.e., increasing the small-signal gain), decreasing intracavity losses, or decreasing the laser-mode and pump-mode size to increase the laser's small-signal gain. Also, lasers with a larger upper-state lifetime and a higher repetition rate show a stronger tendency for self-Q-switching instabilities which was experimentally confirmed with a Nd:YAG ($\tau_2 \approx 250$ μs) and a Nd:YLF laser ($\tau_2 \approx 450$ μs). We have demonstrated previously that a longer carrier lifetime of the A–FPSA increase the tendency for self-Q-switching because $d(\Delta R)/dP_c$ is increased [2]. With the carrier lifetime we can optimize the A–FPSA design for stable cw mode locking even though the working-parameter range is rather small [52].

To obtain a quantitative measure for self-Q-switching we use a photodetector with a microwave spectrum analyzer. In the frequency domain the detected intensity of the mode-locked laser produces harmonics at multiples of the pulse repetition rate and the relaxation oscillations produce noise side bands which peak at the relaxation oscillation frequency with a certain attenuation with respect to the laser harmonic [74–76]. With increasing pump power a solid-state laser with an A–FPSA goes typically through three stages, which are demonstrated with a Nd:YLF laser [1, 2]. First, the A–FPSA produces strong self-Q-switching instabilities with dominant noise side bands around the enhanced axial mode beating-noise peak which later becomes the first-harmonic signal at the pulse-repetition rate (Fig. 16a). No stable pulse formation is observed on any diagnostic system such as autocorrelation and sampling scope. Second, self-Q-switching becomes stable producing typically μs-long envelope pulses or macro pulses over the mode locked pulse train. The self-Q-switching produces very strong modulation side bands (typically around -1 dBc) at around the relaxation oscillation frequency (Fig. 16b). Third, the laser moves into stable cw mode locking with the relaxation oscillation-noise side bands typically ≥ 50 dB below the first harmonic of the mode-locked pulses (Fig. 16c) [2]. The strength of the relaxation oscillation-noise side bands with respect to the first harmonic gives a quantitative measure of how well self-Q-switching instabilities are suppressed and how stable the laser is cw mode-locked. Our experimentally determined condition for the onset of self-Q-switching instabilities is not in agreement with the predicition of (15). This may be explained by the fact, that (15) describes the case of pure Q-switching, whereas we are in the case of both passive mode locking and Q-switching.

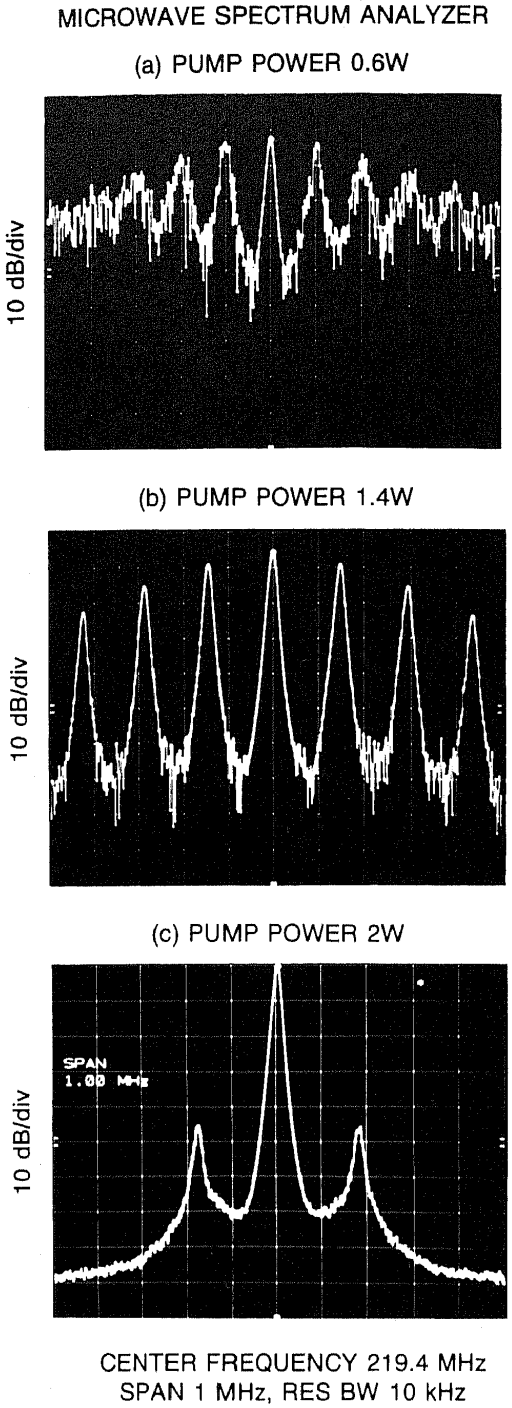

Fig. 16a–c. An A–FPSA mode-locked GE-cavity Nd:YLF laser as a function of pump power monitored on a microwave spectrum analyzer. **a** Self-Q-switching instabilities without any pulse formation, **b** stable self-Q-switching of the mode-locked pulse train with strong modulation side bands at the repetition rate of the Q-switched macro pulses at ≈ 150 kHz, **c** stable cw mode locking at a pulse-repetition rate of 219.4 MHz with an ≈ 50 dB supression of self-Q-switching instabilities

8 Femtosecond Mode-Locking Regime

A Fabry-Perot saturable absorber with a large free spectral range and a rather high top reflector has a negligible group-delay dispersion around antiresonance in the high

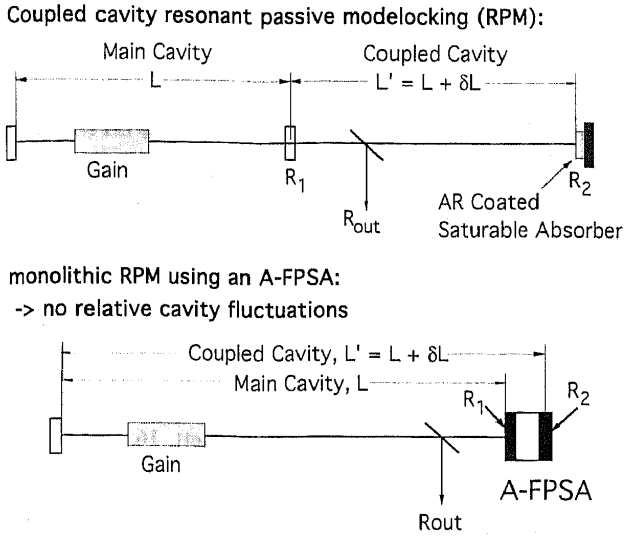

Fig. 17. Coupled-cavity Resonant Passive Mode locking (RPM) is formally equivalent to "monolithic" RPM using an intracavity A–FPSA. An A–FPSA has the advantage that no cavity-length stabilization is required

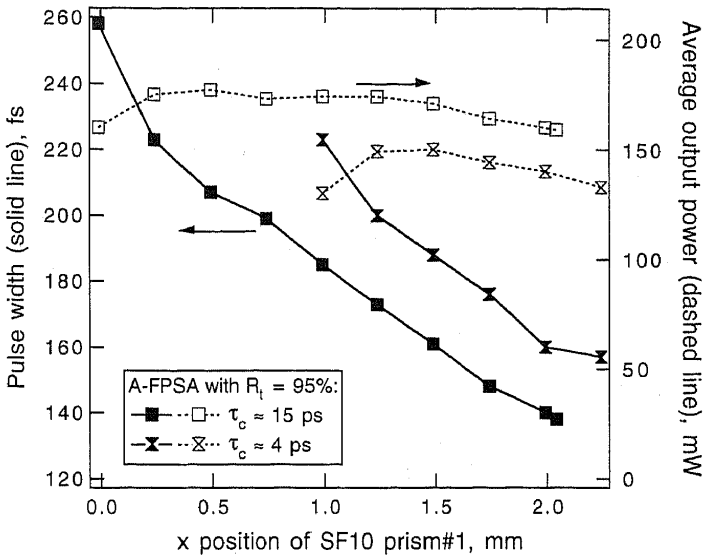

Fig. 18. GM-cavity Nd-doped phosphate glass laser at different dispersion compensation using two SF10 prisms. The pulse width increases with an excess of negative dispersion. A shorter thermalization time of the A–FPSA (Fig. 4f) produces a shorter pulse duration

reflectivity band [50]. Therefore, such an A–FPSA can be used for sub-100 fs pulse generation. The bitemporal A–FPSA (Fig. 4c) in the femtosecond regime both starts mode locking with its slower recovery time constant (Fig. 4d) and supports sub-picosecond pulse durations with its faster recovery time constant (Fig. 4f). Further pulse shortening can be achieved in combination with an even faster saturable absorber such as KLM.

We have demonstrated that RPM can start a KLM Ti:Sapphire laser. In this case, RPM has no effect on the final pulse duration. After the mode locking is started the pulse formation is dominated by KLM because once mode-locked the coupled cavity can be blocked without affecting the femtosecond pulse duration [14, 18]. More recently, similar results were obtained with a KLM Cr:LiSAF laser where RPM was also used as a starting mechanism [73, 77].

We expect to obtain similar results with a correctly designed A–FPSA sample. In fact, modelocking with an A–FPSA is equivalent to "monolithic" RPM (Fig. 17). In this case, the A–FPSA determines the end mirrors for the two coupled cavities that spatially overlap. The top mirror of the A–FPSA forms the end mirror of the main cavity of length L and the dielectric mirror underneath the saturable absorber layer forms the end mirror of the nonlinear coupled cavity of length L'. Because of monolithic integration of these two end mirrors within the same element, no relative cavity length fluctuations exist. Thus, there is no need for an active cavity-length stabilization. Although this formal relation with RPM exists, it is simpler and equally correct to view the entire A–FPSA as an intracavity saturable absorber.

A Nd:glass laser at a lasing wavelength of $\approx 1.05\,\mu m$ has been passively mode-locked with an A–FPSA [5, 78] and pulses as short as 90 fs have been generated [78]. Without negative GVD compensation, the pulse duration was limited to a few picoseconds, shorter than the carrier lifetime but longer than the fast thermalization time of the A–FPSA. In contrast to the results before, where RPM was just used to initiate KLM, the final pulse duration of the Nd:glass laser depends on the A–FPSA sample (Fig. 18). Shorter pulses were generated with an A–FPSA sample with a longer carrier lifetime and a faster thermalization time constant (Fig. 4f). The mode-locking is clearly started by the A–FPSA which produces ≈ 100 times stronger initial mode-locking driving force than KLM. Further work is in progress to study in more detail the different contributions of self-focusing, A–FPSA, self-phase modulation, etc. to the final pulse formation.

Future Directions

From a theoretical point of view there exist well-established mode-locking theories which cover the two limiting cases of mode locking with a fast [63, 64, 79] and slow [47, 80] saturable absorber. The theory of the slow saturable absorber is based on dynamic saturation of the gain medium as an essential part for pulse formation. However, this is not the case for typical solid-state lasers due to their long upper-state lifetimes. Using a bitemporal A–FPSA the usual mode-locking theories do not adequately describe our observed results. Therefore, the existing theories need to be extended.

We plan to extend and demonstrate our A–FPSA mode locking technique to passive mode locking of longer wavelength lasers such as Nd:YAG at 1.3 μm, Er:YAG at $\approx 1.6\,\mu m$, and Tm:YAG at $\approx 2\,\mu m$, for example. The even larger upper-state lifetime of those lasers, typically in the ms regime, will produce an interesting challenge in preventing self-Q-switching instabilities. The sub-100 fs and even sub-10 fs mode-locking regime using an A–FPSA is currently under investigation and will certainly reveal interesting phenomena. Another more applied direction is the development of

compact monolithic mode-locked solid-state lasers which should be now possible with the A–FPSA as a reliable starting and mode-locking force rigidly attached to the laser crystal. In contrast to KLM, the A–FPSA provides a reliable mode-locking driving force over the full stability regime of a laser cavity. This will allow of useful flexibility and reasonable tolerances in the design of compact practical ultrafast-laser sources.

Acknowledgements. This work was mostly done at AT&T Bell Laboratories where U. Keller was a Member of Technical Staff. The author likes to especially thank Heng Chiu from AT&T Bell Laboratories for growing all the semiconductor saturable absorbers, and Luigi Brovelli at the Swiss Federal Institute of Technology for the optical charcterization of the A–FPSA samples, which allowed for the first time a quantitative discussion.

References

1. U. Keller, D.A.B. Miller, G.D. Boyd, T.H. Chiu, J.F. Ferguson, M.T. Asom: Opt. Lett. **17**, 505 (1992)
2. U. Keller, T.H. Chiu, J.F. Ferguson: Opt. Lett. **18**, 217 (1993)
3. K.J. Weingarten, U. Keller, T.H. Chiu, J.F. Ferguson: Opt. Lett. **18**, 640 (1993)
4. M.H. Ober, M. Hofer, U. Keller, T.H. Chiu: Opt. Lett. **18**, 1532 (1993)
5. U. Keller, T.H. Chiu, J.F. Ferguson: Opt. Lett. **18**, 1077 (1993)
6. D. Kopf, F.X. Kärtner, U. Keller: Opt. Lett. (to be published)
7. T.Y. Fan, R.L. Byer: IEEE J. QE-**24**, 895 (1988)
8. S.C. Tidwell, J.F. Seamans, D.D. Lowenthal: Opt. Lett. **18**, 116 (1993)
9. P.F. Moulton: Opt. News Nov./Dec., 9 (1982)
10. P.F. Moulton: J. Opt. Soc. Am. B. **3**, 125 (1986)
11. S.A. Payne, L.L. Chase, L.K. Smith, W.L. Kway, H. Newkirk: J. Appl. Phys. **66**, 1051 (1989)
12. B.H.T. Chai, J.-L. Lefaucheur, M. Stalder, M. Bass: Opt. Lett. **17**, 1584 (1992)
13. W.H. Knox: Opt. Photon. News **3**, 10 (1992)
14. U. Keller, W.H. Knox, G.W. t'Hooft: IEEE J. QE–**28**, 2123 (1992)
15. M.T. Asaki, C.-P. Huang, D. Garvey, J. Zhou, H.C. Kapteyn, M.N. Murnane: Opt. Lett. **18**, 977 (1993)
16. P.F. Curley, C. Spielmann, T. Brabec, F. Krausz, E. Wintner, A.J. Schmidt: Opt. Lett. **18**, 54 (1993)
17. D.E. Spence, P.N. Kean, W. Sibbett: Opt. Lett. **16**, 42 (1991)
18. U. Keller, G.W. t'Hooft, W.H. Knox, J.E. Cunningham: Opt. Lett. **16**, 1022 (1991)
19. D.K. Negus, L. Spinelli, N. Goldblatt, G. Feugnet: In *Advanced Solid-State Lasers,* ed. by G. Dubé, L. Chase, Vol. 10 (Optical Society of America, Washington, DC 1991) pp. 120–124
20. F. Salin, J. Squier, M. Piché: Opt. Lett. **16**, 1674 (1991)
21. K.J. Blow, D. Wood: J. Opt. Soc. Am B **5**, 629 (1988)
22. P.N. Kean, X. Zhu, D.W. Crust, R.S. Grant, N. Landford, W. Sibbett: Opt. Lett. **14**, 39 (1989)
23. E.P. Ippen, H.A. Haus, L.Y. Liu: J. Opt. Soc. Am. B **6**, 1736 (1989)
24. J. Goodberlet, J. Wang, J.G. Fujimoto, P.A. Schulz: Opt. Lett. **14**, 1125 (1989)
25. U. Keller, W.H. Knox, H. Roskos: Opt. Lett. **15**, 1377 (1990)
26. U. Keller, T.H. Chiu: IEEE J. QE–**28**, 1710 (1992)
27. G.W. t'Hooft, U. Keller, W.H. Knox, J.E. Cunningham: Conference on Lasers and Electro-Optics (CLEO) (Optical Society of America, Washington, D,C. 1991) paper JMA6, pp. 6–7
28. J. Son, J.V. Rudd, J.F. Whitaker: Opt. Lett. **17**, 733 (1992)
29. Special issue on optical parametric oscillation and amplification: J. Opt. Soc. Am. B **10**, 2148 (1993)
30. M. Hofer, M.H. Ober, F. Haberl, M.E. Fermann: IEEE J. QE–**28**, 720 (1992)
31. K. Tamura, E.P. Ippen, H.A. Haus, L.E. Nelson: Opt. Lett. **18**, 1080 (1993)
32. K. Tamura, C.R. Doerr, L.E. Nelson, H.A. Haus, E.P. Ippen: Opt. Lett. **19**, 46 (1994)
33. M. Piché, F. Salin: Opt. Lett. **18**, 1041 (1993)
34. J. Harrison, A. Finch, D.M. Rines, G.A. Rines, P.F. Moulton: Opt. Lett. **16**, 581 (1991)
35. V. Magni, G. Cerullo, S.D. Silvestri: Opt. Commun. **96**, 348 (1993)
36. K. Tamura, J. Jacobson, E.P. Ippen, H.A. Haus, J.G. Fujimoto: Opt. Lett. **18**, 220 (1993)
37. G. Cerullo, S.D. Silvestri, V. Magni: Opt. Lett. **19**, (1994) (to be published)
38. N. Sarukura, Y. Ishida, H. Nakano: Opt. Lett. **16**, 153 (1991)
39. J.-C. Kuo, J.-M. Shieh, C.-D. Hwang, C.-S. Chang, C.-L. Pan, K.-H. Wu: Opt. Lett. **17**, 334 (1992)
40. J.D. Kafka, M.L. Watts, J.-W.J. Pieterse: IEEE J. QE–**28**, 2151 (1992)
41. P.F. Curley, A.I. Ferguson: Opt. Lett. **16**, 1016 (1991)
42. D.E. Spence, J.M. Evans, W.E. Sleat, W. Sibbett: Opt. Lett. **16**, 1762 (1991)
43. Y.M. Liu, K.W. Sun, P.R. Prucnal, S.A. Lyon: Opt. Lett. **17**, 1219 (1992)
44. C. Spielmann, F. Krausz, T. Brabec, E. Wintner, A.J. Schmidt: Opt. Lett. **16**, 1180 (1991)
45. Y. Silberberg, P.W. Smith, D.J. Eilenberger, D.A.B. Miller, A.C. Gossard, W. Wiegmann: Opt. Lett. **9**, 507 (1984)
46. P.W. Smith, Y. Silberberg, D.A.B. Miller: J. Opt. Soc. Am. B **2**, 1228 (1985)
47. H.A. Haus, Y. Silberberg: J. Opt. Soc. Am. B **2**, 1237 (1985)
48. M.N. Islam, E.R. Sunderman, C.E. Soccolich, I. Bar-Joseph, N. Sauer, T.Y. Chang, B.I. Miller: IEEE J. QE–**25**, 2454 (1989)
49. T.H. Chiu, U. Keller, M.D. Williams, M.T. Asom, J.F. Ferguson: J. Electron. Mater. (1994) (submitted)
50. L.R. Brovelli, U. Keller: J. Opt. Soc. Am. B **11**, (1994) (submitted March 1994)
51. F. Gires, P. Tournois: C. R. Acad. Sci. Paris **258**, 6112 (1964)
52. H.A. Haus: IEEE J. QE–**12**, 169 (1976)
53. Y. Tsou, E. Garmire, W. Chen, M. Birnbaum, R. Asthana: Opt. Lett. **18**, 1514 (1993)
54. Z. Zhang, L. Qian, D. Fan, X. Deng: Appl. Phys. Lett. **60**, 419 (1992)
55. G.P.A. Malcolm, A.I. Ferguson: Opt. Lett. **16**, 1987 (1991)
56. K.X. Liu, C.J. Flood, D.R. Walker, H.M. v. Driel: Opt. Lett. **17**, 1361 (1992)
57. U. Keller, K.J. Weingarten, K.D. Li, D.C. Gerstenberger, P.T. Khuri-Yakub, D.M. Bloom: Opt. Lett. **15**, 45 (1990)
58. K.J. Weingarten, D.C. Shannon, R.W. Wallace, U. Keller: Opt. Lett. **15**, 962 (1990)
59. G.T. Maker, A.I. Ferguson: Appl. Phys. Lett. **54**, 403 (1989)
60. A.A. Godil, A.S. Hou, B.A. Auld, D.M. Bloom: Opt. Lett. **16**, 1765 (1991)
61. B. Braun, K.J. Weingarten, U. Keller: Accepted Poster at CLEO 1994, paper CThI1
62. F. Krausz, T. Brabec: Opt. Lett. **18**, 888 (1993)
63. H.A. Haus: J. Appl. Phys. **46**, 3049 (1975)
64. H.A. Haus, U. Keller, W.H. Knox: J. Opt. Soc. Am. B **8**, 1252 (1991)
65. J. Goodberlet, J. Wang, J.G. Fujimoto, P.A. Schulz: Opt. Lett. **15**, 1300 (1990)
66. N. Sarukura, Y. Ishida: Opt. Lett. **17**, 61 (1992)
67. J.-C. Kuo, C.-L. Pan: Opt. Lett. **15**, 1297 (1990)
68. K.J. Weingarten, B. Braun, U. Keller: Opt. Lett. (submitted)
69. A.E. Siegman: *Lasers* (Univ. Science Books, Mill Valley, CA 1986)
70. R. Adair, L.L. Chase, S.A. Payne: Phys. Rev. B **39**, 3337 (1989)
71. G.J. Quarles: Lightning Optical Corp., (private communication)

72. V.P. Mikhailov, Q.Z. Wang, M. Chu, J.M. Buchert, R.R. Alfano: Appl. Opt. **32**, 3944 (1993)
73. N.H. Rizvi, P.M.W. French, J.R. Taylor, P.J. Delfyett, L.T. Florez: Opt. Lett. **18**, 983 (1993)
74. D. v. d. Linde: Appl. Phys. B **39**, 201 (1986)
75. M.J.W. Rodwell, K.J. Weingarten, D.M. Bloom, T. Baer, B.H. Kolner: Opt. Lett. **11**, 638 (1986)
76. U. Keller, K.D. Li, M.J.W. Rodwell, D.M. Bloom: IEEE J. QE–**25**, 280 (1989)
77. P.M.W. French, R. Mellish, J.R. Taylor: Opt. Lett. **18**, 1934 (1993)
78. F.X. Kärtner, D. Kopf, U. Keller: Ultrafast Phenomena (1994), 9th Int'l Meeting, accepted for oral presentation (paper MA5)
79. H.A. Haus, J.G. Fujimoto, E.P. Ippen: IEEE J. QE–**28**, 2086 (1992)
80. H.A. Haus: IEEE J. QE–**11**, 736 (1975)
81. J.A. Valdmanis, R.L. Fork: IEEE J. QE–**22**, 112 (1986)
82. R.L. Fork, C.H.B. Cruz, P.C. Becker, C.V. Shank: Opt. Lett. **12**, 483 (1987)